2015

Measurement of Formic and Acetic Acid in Air by Chemical Ionization Mass Spectroscopy: Airborne Method Development

Victoria Treadaway
University of Rhode Island, vtreada@my.uri.edu

MEASUREMENT OF FORMIC AND ACETIC ACID IN AIR BY CHEMICAL IONIZATION MASS SPECTROSCOPY: AIRBORNE METHOD DEVELOPMENT

BY

VICTORIA TREADAWAY

A THESIS SUBMITTED IN PARTIAL FULFILLMENT OF THE REQUIREMENTS FOR THE DEGREE OF

MASTER OF SCIENCE

IN

OCEANOGRAPHY

UNIVERSITY OF RHODE ISLAND

2015

MASTER OF SCIENCE THESIS

OF

VICTORIA TREADAWAY

APPROVED:

Thesis Committee:

Major Professor Brian Heikes

John Merrill

James Smith

Nasser H. Zawia
DEAN OF THE GRADUATE SCHOOL

UNIVERSITY OF RHODE ISLAND
2015

ABSTRACT

The goals of this study were to determine whether formic and acetic acid could be quantified from the Deep Convective Clouds and Chemistry Experiment (DC3) through post-mission calibration and analysis and to optimize a reagent gas mix with CH_3I, CO_2, and O_2 that allows quantitative cluster ion formation with hydroperoxides and organic acids suitable for use in future field measurements. There is a scarcity of organic acid measurements in the upper troposphere under stormy conditions with which to compare and assess photochemical and transport theory. DC3 observations made in May and June 2012 extending from the surface to 13 km over the central United States during convective storm conditions would be a significant addition to our knowledge base. Organic acid measurements were made with a chemical ionization mass spectrometer (CIMS) aboard the NCAR Gulfstream-V platform in DC3. The primary objective of the CIMS was to observe hydrogen peroxide and methyl hydroperoxide though it recorded signals attributed to iodide clusters of formic and acetic acid at 173 and 187 townsend, respectively. Both organic acids were targets of opportunity as the reagent ion (I^-) needed for clustering was not specifically used in the field. However an iodide source gas (iodomethane, CH_3I), was used during pre-mission experiments and a residual amount adsorbed onto the inlet surfaces was found to be bleeding off the plumbing in the field. Post-mission laboratory experiments were performed to determine the CIMS instrument's sensitivity to these organic acids under iodomethane outgassing and the varying water vapor and sample flow conditions encountered during DC3 flights. Laboratory calibration experiments with varying iodomethane concentrations, inlet pressures, and water vapor mixing ratios

were performed. Calibrations for hydrogen peroxide and methyl hydroperoxide were used to tune the reagent gas mixture composed of CH_3I, CO_2, and O_2 to best match the observed sensitivities for hydrogen peroxide and methyl hydroperoxide in DC3. Formic and acetic calibration functions were fit to the water vapor and sample flow results. Formic acid displays both a water vapor and inlet pressure dependence, whereas, acetic acid sensitivity was found to be independent of water vapor and inlet pressure within the range of conditions encountered in DC3 and the laboratory. These laboratory calibrations were further evaluated by comparison to in-flight calibrations from the Front Range Air Pollution and Photochemistry Experiment (FRAPPE) to confirm the reliability of the fits and laboratory methodology. The laboratory and field calibration work showed very good correspondence for hydrogen peroxide, methyl hydroperoxide, and acetic acid. However, the apparent formic acid sensitivity fits gave a factor of two greater sensitivity than observed in the FRAPPE formic acid field calibrations. Further comparison to ground and prior airborne measurements suggest the calibration problem lies in the FRAPPE field calibration and the laboratory work was valid for formic acid as it was for DC3 and FRAPPE peroxides and FRAPPE acetic acid. Subsequently, the laboratory calibration fits were applied to quantify DC3 formic and acetic acid. A DC3 research flight (RF 03) case study is presented to illustrate formic and acetic acid behavior when air from a high biogenic source region with identifiable convective storm outflow was sampled.

ACKNOWLEDGMENTS

I would like to thank Brian Heikes who has supported me through this whole process and provided much needed guidance through the many unanticipated roadblocks we encountered. You have opened me up to a world I didn't even know existed and as frustrating as "out of the beaker" chemistry is I wouldn't change it for anything. Thanks to Dan O'Sullivan for your support and for being my pseudo second advisor. I would also like to thank my committee for their insight and support as well through this process. None of this would be possible without the fellow scientists and the "mechs and techs" from both DC3 and FRAPPE. Atmospheric chemistry is truly a group adventure and without each person it would like trying to solve a puzzle without all the pieces.

I would also like to thank the many friends I have made in Rhode Island. I could not have made it through this without your support, distractions, advice, coffee runs, Netflix binges, and Brickley's ice cream trips in the summer. I have been lucky to meet each of you and now you are stuck with me forever.

Finally, I would like to thank my family. They have stood by me from the beginning and supported my choice to move across the country to do science. My parents have provided insight and guidance in the way that only parents can and have kept me tethered to reality by reminding me what is really important. Last, but never least, to my brother who no matter how far apart we are it is like no time passed when we are together and I know you always have my back. Here is an official in writing promise to one day go to SDCC.

TABLE OF CONTENTS

LIST OF TABLES

TABLE PAGE

LIST OF FIGURES

FIGURE PAGE

1. INTRODUCTION

Formic acid (HFo) and acetic acid (HAc) have both natural and anthropogenic sources. A representation of the biogeochemical cycle of HFo and HAc is shown in Figure 1 and some of the major sources are discussed here. Primary emissions for both include biomass burning, biogenic sources, and motor vehicles (Khare et al. 1999; Paulot et al. 2011). Secondary production is a significant source for both acids especially from biogenic precursors, secondary organic aerosols, and photochemical production from volatile organic compounds (VOCs) and oxygenated volatile organic compounds (OVOCs) (Khare et al. 1999; Paulot et al. 2011). For example, an indirect VOC source of HFo is the ozonolysis of isoprene which is released naturally by vegetation (Khare et al. 1999). Models, laboratory work, and field measurements agree that the ozonolysis of isoprene is a significant source of HFo (Khare et al. 1999). The oxidation of other biogenic compounds will also release both acids. Unfortunately, a great deal of uncertainty remains concerning the yield and mechanisms of these *in situ* chemical reactions although the critical component is the source strength and fate of the Criegee biradical from alkene ozonolysis

$$RC{=}CH_2 + O_3 \rightarrow RCHO + HCOO^-$$

(Millet et al. 2015).

Biomass burning provides an important primary and secondary source of both acids to the atmosphere. HAc has a larger direct source from biomass burning than HFo (Paulot et al. 2011). Most HFo and HAc produced in biomass plumes occur via secondary production from VOC precursors. Both organic acids have been measured as primary emissions in motor vehicular exhaust with greater HAc relative to HFo

(Kawamura, Ng, and Kaplan 1985). It is hypothesized that both organic acids are released as a result of incomplete combustion which is supported by the high organic acid concentration measured in used oil (Kawamura, Ng, and Kaplan 1985).

Secondary organic aerosols are another potential source for HFo and HAc, though this is a poorly quantified production pathway. The role of organic acids in secondary organic aerosol (SOA) aging has become more widely recognized and studied in the last ten years. SOAs are formed by the chemical transformation of atmospheric organic compounds through oxidation of gas-phase species (Fuzzi and Andreae 2006). Photochemical aging alters the physical and chemical properties of aerosols in the atmosphere (Fuzzi and Andreae 2006). Field studies (INTEX-B and ARCPAC 2008) generated data that support a positive correlation between HFo and HAc production and organic aerosol aging in the atmosphere. It is hypothesized that SOA aging releases both acids into the atmosphere. Current models underestimate the level of HFo and HAc especially when there are no large biogenic or anthropogenic sources nearby (Paulot et al. 2011). For example, HFo and HAc measured in Asian air masses sampled during INTEX-B were expected to have lower concentrations due to scavenging; however, both acids were present at high concentrations which indicates that there must have been a secondary source for both acids (Paulot et al. 2011; Dunlea et al. 2009). SOA production of these acids could account for the gap between modeled and observed concentrations. Paulot et al. (2011) remark that there is a positive correlation between the concentration of HFo and the level of aerosols present. These data help support the hypothesis that organic acids are released or co-formed during the aerosol formation and aging process. Similar evidence was

collected during ARCPAC 2008, which showed the relationship between HAc and black carbon along with aerosol organic content. This work indicated a potential missing precursor for HFo and HAc coupled with biomass burning (Paulot et al. 2011). Until the recent advancement in measurement technology, it was difficult to measure these aging processes due to the short time scale over which they occur. Current atmospheric models cannot explain the magnitude and evolution of atmospheric SOAs. Paulot et al.'s (2011) comparison of model and field measurements found that models may be underestimating the concentrations of both organic acids by up to 50%. More accurate measurements of HFo and HAc in the atmosphere would contribute to our understanding of SOA aging processes and improve atmospheric models.

HFo and HAc have the potential to be used as convective transport tracers. The water solubility for both acids is dependent on the pH due to dissociation. Below pH 4, HAc is more soluble than HFo (Pandis and Seinfield 2006). Above pH 4, HFo is more soluble because it has a more efficient dissociation (Pandis and Seinfield 2006). Barth et al. (2007) modeled various mid-latitude storms for peroxides and HFo. Hydrogen peroxide (HP) and methyl hydroperoxide (MHP) are used as deep convective transport tracers (Barth et al. 2007; Snow et al. 2007). HP has a higher Henry's Law constant ($H = C_{aq}/P$) than MHP (O'Sullivan et al., 1996); therefore, HP will be removed in a storm cloud preferentially via wet deposition. Very little MHP was scavenged in Barth et al.'s (2007) modeled storms: about 7%. Barth et al. (2007) found that HFo in modeled convective outflow was small when assuming the initial aqueous and gas-phase concentrations were zero. However, the amount of HFo present depends on the

storm type (affecting aqueous phase HFo production) and cloud and rainwater pH (Barth et al. 2007). The majority of HFo formed in clouds is in the aqueous phase. Barth et al. (2007) determined that it may be possible to use HFo to detect cloud-processed air though it is highly dependent on cloud conditions and the initial concentration of HFo. Unfortunately, there is minimal observational literature using HFo and HAc as deep convective system transport tracers.

Measurements reported here were obtained using a newer analytical technique for atmospheric measurements known as chemical ionization mass spectrometry (CIMS). The major advantages of using CIMS are the rapid response time and increased sensitivity (Crounse et al. 2006; Messer et al. 2000). CIMS directly measures chemical species of interest based upon the molecule's mass-to-charge ratio (m/z) and can rapidly monitor and alternate between several mass-to-charge ratios. A faster sampling rate makes it possible to detect reactions on the storm scale (10s to 100s of meters). The CIMS individual m/z sampling rate is about 0.1 s^{-1} but it takes about 1 s to sample all selected m/z values. These rates correspond to distances of 0.02 - 0.2 km for an aircraft traveling at 200 m/s, such as the G-V used in DC3, and the horizontal scale of a deep convective storm is on the order of 10 km. While CIMS instruments have been used to measure many trace atmospheric species, there have been limited measurements of peroxides and organic acids.

A recent example of airborne measurements for HFo using CIMS was performed by Le Breton et al. (2012). They reported one flight day worth of data and measured HFo mixing ratios between 34.4 pptv and 358 pptv with an average of 142.4 pptv (Le Breton et al. 2012). This was an informative study because they were able to

distinguish three different urban plumes with elevated levels of HFo. This work highlights the ability of CIMS to perform rapid, sensitive measurements in-flight. This thesis expands Le Breton's iodide reagent chemistry work to both HFo and HAc.

HP and MHP were target species of interest measured using CIMS during the Deep Convective Clouds and Chemistry (DC3) campaign in 2012. DC3 focused on studying atmospheric chemistry and transport under deep convective storm conditions in the central and eastern United States. Prior to the DC3 mission, an initial mixture of CH_3I in nitrogen (unknown mixing ratio) was used in the peroxide CIMS instrument. This reagent mixture did not produce an ion for the measurement of MHP and was discontinued before DC3. A second mixture composed of CO_2 in pure air and blended with pure nitrogen was tested. This reagent mix yielded ion signals for HP and MHP clusters with $CO_2 \bullet O_2^-$ and O_2^-, respectively. At the start of DC3, it was observed that ambient air samples gave significant signals at the ion cluster masses corresponding to 173 ($I^- \bullet HCOOH$) and 187 ($I^- \bullet CH_3COOH$) townsend. It was discovered that residual CH_3I was bleeding off the reagent gas plumbing and acting as a dilute source of I^-. Normal reagent CH_3I gas concentrations used in CIMS are sufficient to suppress O_2^- ion chemistry. Fortuitously, the residual CH_3I was suitable to allow O_2^-, $CO_2 \bullet O_2^-$ and potentially I^- ion chemistries to be used simultaneously. Therefore, iodide cluster masses for I^-, $I^- \bullet H_2O$, $I^- \bullet H_2{}^{18}O$, $I^- \bullet H_2O_2$, $I^- \bullet HCOOH$, and $I^- \bullet CH_3COOH$ were monitored during DC3. The expectation was post-mission laboratory calibrations could be developed permitting quantification of the organic acid mixing ratios. The goal of this work was two-fold: determine HFo and HAc sensitivities encountered during DC3 and optimize a reagent gas mix with CH_3I, CO_2,

and O_2 that allows the clustering of both peroxides and both organic acids to be used in future field measurements.

2. METHODS

2.1 Instrumental Configuration

Continuous gas analysis was performed using a chemical ionization mass spectrometer (THS Instruments, Inc., Atlanta, GA). The chemical ionization mass spectrometer (CIMS) is adapted for peroxides and organic acids and is used in a negative ion mode. This thesis focuses on HFo and HAc, which form cluster ions with the iodide reagent ion, I^-, at 173 (I^-•HCOOH) and 187 (I^-•CH_3COOH) townsend, respectively. The CIMS normally operates in a "hop" mode, whereby specific mass-to-charge ratios are sampled sequentially. The sample and analytical system is depicted schematically in Figure 2. Critical system elements include: gas delivery inlet with calibration system, the CIMS, exhaust lines, and a data acquisition and control system. The CIMS is further composed of an ion generation and reaction system, ion selection (declustering ion guide and quadrupole), multi- ion counting detector, controlling electronics, and vacuum pump system.

Ambient, or sample, air enters the CIMS system through a PFA Teflon inlet. In the laboratory, synthetic air mixtures are delivered to the inlet. In airborne field work, the inlet is external to the fuselage and aerodynamically designed to minimize the collection, volatilization, and subsequent analysis of large aerosol and droplet material. The inlet is heated to minimize artifacts by the adsorption of the target gases onto the inlet walls. Calibrations are performed by standard addition to the sample air stream. The calibration gas flows continuously and a "draw-back" design is employed

to modulate between sample air and sample air with calibration gas added. In the "draw-back" mode a 2-way valve is opened and a pump, regulated by a mass flow controller (MFC), pulls the calibration gas flow and a small excess flow of sample air to waste. In this configuration sample air without standard is measured. When the valve is closed, the "draw-back" is off and calibration gas is added to the sample air stream. A detailed discussion of the different calibration set-ups is given in Section 2.3. Analytical blanks are determined by passing the sample air stream, with or without calibration gas, through an organic acid trap. A three-way solenoid valve is used to select between the sample air stream or sample air after passing through the trap. A description of the different traps tested is in Section 2.4. Last the inlet flow is split with a portion being pumped to waste and the remainder is introduced to the CIMS system. The excess sent to waste is used to increase the sample volume relative to the plumbing surface area which minimizes instrumental material effects on the sample.

In the CIMS, the sample air passes through a series of chambers to form, select, and quantify the organic acid ion clusters. The first chamber is the ion-sample reaction cell, RXN in Figure 2. In the reaction cell, the sample air is mixed with a reagent ion stream (discussed fully in Section 2.5) of which the bulk is pure nitrogen and controlled by MFCs. The reagent gas passes through a commercial electrostatic eliminator (NRD, Inc., Grand Island, NY) which contains 20 mCi of ^{210}Po, an alpha emitter, and thus develops the requisite reagent ion stream. Sample air is introduced into the reaction cell through a critical orifice. The sample-reagent ion stream is pumped out of the RXN cell through a second critical orifice into the collisional

dissociation chamber, CDC in Figure 2, which breaks apart weak ion clusters in order to lower background signal counts. The remaining ion clusters are mass filtered and counted by a quadrupole mass spectrometer and multi-channel ion detector.

In this work both the sample-in and exit critical orifices were of fixed diameter. The gas volume flow rate across an orifice depends upon the area of the orifice and the pressure differential across the orifice. Upstream of the inlet orifice the pressure is at ambient level. Downstream of the outlet orifice the pressure is effectively zero. The manufacturer (THS Instruments, Inc., Atlanta, GA.) optimized the CIMS orifice areas to have a reaction cell pressure of 22 hPa given the vacuum pump system. This provides the maximum yield of cluster ions and peak sensitivity and was not further evaluated. Reaction cell pressure is measured and actively controlled at 22 hPa by manipulating the pure nitrogen flow rate of the reagent stream. For groundwork with relatively constant ambient pressure in the inlet, the reagent nitrogen and the sample flow rates are effectively constant and nominally 2.0 and 2.8 slpm (standard liters per minute at T = 273.15 K and P = 1013.25 hPa), respectively. However in airborne operations, the inlet pressure decreases with altitude as does the sample flow rate into the RXN chamber, and it is necessary to increase the reagent nitrogen flow rate to maintain a constant pressure within the CIMS flow sections. The effect of sample inlet pressure or sample flow rate on instrument response was examined in the laboratory (Section 2.2). For future airborne work, the sample fixed size critical orifice will be replaced by a variable size orifice which will maintain constant sample and reagent gas flow rates.

2.2 Laboratory Set-up

In the laboratory different field conditions are simulated by varying the water vapor and/or the inlet pressure of the sample air stream as depicted in Figure 3. A zero air generator (Aadco Instruments Inc., Cleves, OH) supplies the sample air stream to prevent the addition of organics and excess water into the system. This air stream is split between dry and humidified lines. The dry line comes directly from the Aadco. The water concentration in the humidified line is controlled with two gas washing bottles and a gas-water equilibration coil immersed in a water bath kept routinely at 288 K (Figure 4). By changing the ratio of air flow through the dry and humidified lines, it is possible to alter the overall water vapor in the air stream entering the CIMS. Most laboratory work was done with the coil water bath at 288 K which gives a maximum reaction cell water vapor mixing ratio of 4500 ppm. Normal room temperature is controlled at 293 K. Higher humidity work was performed to expand the reaction cell water vapor mixing ratio range to 7800 ppm for comparison to literature data (Lee et al. 2014; Baasandorj et al. 2014). The temperature in the coil water bath was raised to 298 K and the laboratory room temperature was increased to 303 K to prevent the water vapor from condensing on the tube walls (Thanks to Dallas Hazard).

The inlet pressure is controlled after the humidification with a needle valve (P, Figure 3) and a pressure transducer. The needle valve is able to approximate the atmospheric altitude conditions (sea level to 14 km, approximately 120 hPa) experienced in the field. The sample flow rate changes as a function of altitude (ambient pressure) which will impact the signal response and sensitivity.

2.3 Calibration Configuration

The HFo and HAc standards (HCOOH, $\geq$ 95% and CH_3COOH, 99.9%, respectively) were obtained from Sigma-Aldrich. There is a <1% HAc impurity in the HFo standard and 2.0-2.5% water for stabilization. Laboratory prepared microfluidic and coil aqueous standards were not standardized against a primary reference material. In FRAPPE microfluidic aqueous standards were verified by titration against sodium hydroxide (Santa Monica College 2014). The percent errors between the theoretical and titrated concentrations for FRAPPE were 1.00% and 1.51% for HFo and HAc, respectively. The sensitivities are reported with three significant figures (Table 2) for all work as a result of this small error. The FRAPPE aqueous standards were titrated post-mission (2 months later) as well. The standard solutions did not decay substantially with time. There was a 1.91% and 3.67% percent decrease in concentration by the end of the campaign for both HFo and HAc.

Calibrations were performed with coil or microfluidic injection. The laboratory coil calibration system (Figure 5a) allowed the organic acids to be added in the sample air stream prior to entering the CIMS. Zero air (200 or 400 sccm) was passed through a glass coil in a water bath (nominally 288 K) along with the liquid organic acid standard. HFo (0.3 mM) and HAc (0.9 mM), were acidified (0.02 N H_2SO_4) to keep each acid in its protonated form and thereby ensure partitioning into the gas phase according to each acid's Henry's Law constant. The calibration gas was added to the sample air stream after humidification. The higher humidity work was done with the coil calibration system; therefore, the calibration coil temperature was increased to 298 K. The Johnson et al. (1996) temperature dependent Henry's Law constants were

chosen because they provided the closest relationship between the microfluidic and coil work. The Henry's Law constants for HFo are 17.87 and 8.79 M/hPa at 288 and 298 K, respectively (Johnson, Betterton, and Craig 1996). The Henry's Law constants for HAc are 8.43 and 4.05 M/hPa at 288 and 298 K, respectively (Johnson, Betterton, and Craig 1996).

Two versions of the microfluidic system were used to inject the liquid standard into the CIMS via nitrogen gas line. For the first set-up (Figure 5b) the standard, an aqueous HFo and HAc mixture (1 mM each), contained in a Hamilton glass syringe was injected using a single syringe pump (1×10^{-6} L/min aqueous flow rate, KD Scientific Inc., Holliston, MA). The liquid standard was vaporized in a heating block (328 K) into a gaseous N_2 stream (0.4 slpm). The disadvantage of this system is that it can only calibrate for peroxides or organic acids. In DC3, a single syringe was used and the priority measurements were the peroxides. After DC3, a second system (Figure 5c) was set up which allows for calibration of peroxides and organic acids. Both peroxide and organic acid standards are evaporated into a N_2 gas stream (0.4 slpm) via mixing-Ts and equilibrated in a mixing jar. This system uses two syringes; therefore, the flow rate is halved (500×10^{-9} L/min) and the aqueous concentrations of the organic acids are doubled (2 mM) to prevent water saturation of the N_2 gas while maintaining a similar reaction cell sensitivity factor (Section 2.8). Both microfluidic standard addition systems can be contained within the CIMS instrument rack. In-flight calibrations were done as part of the FRAPPE program (Section 2.7) in the summer of 2014 with the second microfluidic set-up. These standard additions along with laboratory calibrations are used to reduce organic acid data for DC3.

2.4 Blank Configuration

The laboratory blank work used either a Carulite-200® trap or Aadco zero air. Carulite-200® (Carus Corporation, Peru, IL), a magnesium dioxide/ copper oxide catalyst, is an effective ozone and peroxide destruction catalyst. It further proved to be effective in removing but not destroying the organic acids as well. Unfortunately at low organic acid concentrations there can be a positive trap response due to outgassing from the Carulite-200®. For some laboratory experiments Aadco air was used to represent the blank as it is free of organic acids.

During FRAPPE (Section 2.7) three different traps were tested for organic acids: Cu/$NaHCO_3$, Na_2CO_3, and NaOH. The Cu/$NaHCO_3$ trap scrubbed the organic acids and HP but generated a positive trap response at 80 townsend which is monitored for MHP. It is possible that the trap was releasing ozone ($O_3 \cdot O_2$) or a MHP hydrocarbon precursor which is also at 80 townsend. The Carulite 200® trap was added after the Cu/$NaHCO_3$ trap which successfully eliminated the positive trap response at 80 townsend. While this trap configuration removed both peroxides and organic acids the HAc equilibration time was too long for inflight blanks. The HAc blank did not level out over the 90 second blank. The NaOH (5%) trap only removed organic acids. Running the air sample through the Carulite 200® and then the NaOH trap removed both peroxides and organic acids with limited outgassing. The blank equilibration time (30-45 seconds) was much shorter than with the Carulite 200® and Cu/$NaHCO_3$ trap. The Na_2CO_3 trap is a mixture of sodium carbonate (5 g), glycerol (5 g), water (250 mL), and methanol (250 mL) based on the EPA SOP (EPA 2009). This trap was tested with and without the NaOH trap. Unfortunately, there was an

outgassing of compounds which interfered at the masses used to measure HAc and HP; possibly from contaminants in the glycerol or methanol used to prepare the trap or from *in situ* chemical reactions leading to HAc and/or HP production on the Na_2CO_3 trap. One example is

$$CH_3OOH + CH_3CO \rightarrow CH_3C(O)OH + CH_3O^{\bullet}$$

which could lead to the formation of HAc in the trap (Hermans, Jacobs, and Peeters 2007). It is also possible that an isomer was formed such as glycolaldehyde which has the same molecular weight as HAc.

2.5 Reagent Gas

The iodomethane (CH_3I) reagent gas laboratory calibrations were performed using two different mixing ratios of CH_3I in N_2. The initial iodomethane mixture (0.33% in N_2) was prepared similarly to Le Breton et al.'s work (2012) with the exception water vapor was not added. The dynamic range of the iodomethane MFC was insufficient to reduce the iodomethane concentration of the "Le Breton" mixture enough to represent DC3 as O_2^- ion signals were too small. The 0.33% iodomethane mixture was then serially diluted twice with N_2 gas – first to 0.025% and then to 5 ppm. The latter dilution was used with a MFC to prepare custom reagent gas blends of CH_3I, CO_2, O_2, and N_2 sufficient to yield responses for both I^- and O_2^- cluster ions which overlapped those observed in DC3. A mixing cross was used to blend the CO_2 in air (400 ppm), the CH_3I in N_2 (5 ppm), and the pure N_2 reagent gases (Table 1). Each gas flow was controlled via MFCs.

Calibrations at the different inlet pressures and specific humidities were performed. The CO_2 in air mass flow rate was held constant at 0.080 slpm. The 5

ppm CH_3I mixture was added at 5 different flow rates ranging from 0.0005 to 0.0025 slpm in 0.0005 slpm increments. Table 1 lists the CH_3I, CO_2, and O_2 mixing ratios in N_2 of the reagent gas blend as a function of CH_3I mass flow rate and inlet pressure (recall N_2 flow varies with inlet pressure to maintain a constant reaction cell pressure). This made it possible to explore how changing CH_3I will impact the signal response of both peroxides and both organic acids. During the variable CH_3I experiments, blanks were performed using the Aadco system. For each inlet pressure (120, 180, 360, 600, and 1013 hPa), the different CH_3I flow rates were all performed in one day to avoid daily instrumental variance.

2.6. Deep Convective Clouds and Chemistry Experiment

The Deep Convective Clouds and Chemistry (DC3) field campaign was conducted in the central United States from May 18 to June 30, 2012 and took advantage of semi-permanent research weather radars in Colorado, Texas/Oklahoma, and Alabama. Details regarding the DC3 science objectives and plan are available at UCAR EOL (http://www.eol.ucar.edu/field_projects/dc3) and the data archive is available at UCAR EOL (http://data.eol.ucar.edu/master_list/?project=DC3). The CIMS was onboard the NCAR Gulfstream-V (GV) which flew 22 research flights. Our primary chemical species of interest in the field were HP and MHP; however, raw data are available for HFo and HAc as well. A total of three aircraft participated in the campaign: the German Aerospace Center (DLR) Falcon, the NASA DC-8, and the GV. Ancillary chemical and meteorological date are used to interpret the HFo and HAc measurements from the GV.

The reagent gas during DC3 was CO_2 (400 ppm, 0.080 slpm) in ultrapure air blended with pure N_2. The CO_2•O_2 reagent gas optimized the HP and MHP signal response (O'Sullivan, personal communication, January 2012). Procedural blanks were obtained using a Carulite 200® trap. HP and MHP calibrations were performed using the single syringe microfluidic system described in Section 2.3. The solution standards were 5.7 mM for HP and 4.8 mM for MHP and the syringe flow rate was 1 x 10^{-6} L/min.

2.7 Front Range Air Pollution and Photochemistry Experiment

The Front Range Air Pollution and Photochemistry Experiment (FRAPPE) consisted of 15 research flights over the northern Colorado Front Range from July 17 to August 18, 2014. The CIMS was flown on the NCAR C-130 as part of a multi-platform campaign. Details regarding the FRAPPE science objectives and plan are available at UCAR EOL (https://www.eol.ucar.edu/field_projects/frappe) and the data archive is available at NASA Data Archive (https://www-air.larc.nasa.gov/cgi-bin/ArcView/discover-aq.co-2014?C130=1). FRAPPE was the first campaign using the two-syringe microfluidic calibration system and three-mixture blended reagent ion scheme. The CO_2 (400 ppm, 0.080 slpm) in ultrapure air was mixed with CH_3I (5 ppm in N_2, 0.0005 slpm) into the N_2 stream. The peroxide calibrations were performed with a mixed standard of HP (15.9 mM), MHP (14.9 mM), and isotopically labeled MHP (CD_3OOH, 14.9 mM). The organic acid calibrations were performed with a mixed HFo (5.88 mM) and HAc (5.88 mM) standard. The syringe flow rates were each 325 x 10^{-9} L /min. Three different trap sets were used during FRAPPE to determine procedural blanks (see Section 2.4). RF01 through RF05 and RF07 used

only the Carulite 200® trap. RF06 used the Carulite 200® and $NaHCO_3$ trap in series. RF08 through RF 15 used the Carulite 200® and NaOH traps in series. The latter provide the best combination of peroxide and organic acid blanks.

2.8 Data Analysis

The organic acid reaction cell mixing ratios (sensitivity factors) were calculated for both the peroxides and organic acids. The reaction cell pressure was kept constant at 22 hPa. The cell temperature was between 298 and 308 K as randomly checked during flight and in the laboratory. These mixing ratios or concentrations are directly proportional and mixing ratio was simply used as the analyte measure of choice. For standard addition using the coil equilibration sources, the reaction cell mixing ratio is given by:

$$X_{\text{coil rxncell}} = \left(\frac{C/H}{P_{1013}}\right) * \left(\frac{F_c}{F_{\text{Aadco}}}\right) * \left(\frac{F_{\text{sample}}}{F_{\text{CIMS}}}\right) \quad (1)$$

where C is the aqueous concentration of the standard in the coil (molar, M), H is the Henry's Law constant (M / hPa), P_{1013} is the coil reference pressure (1013 hPa), F_c is the mass flow rate of air through the coil (slpm), F_{Aadco} is the total flow (slpm) through the inlet prior to the inlet pressure valve, F_{sample} is the mass flow rate across the reaction cell critical orifice (slpm), and F_{CIMS} is the mass flow rate across the reaction cell outlet critical orifice (4.68 slpm). F_{sample} is calculated by difference by subtracting the reagent gas and N_2 mass flow rates from F_{CIMS}.

Alternatively when using the microfluidic addition system, the standard gas mixing ratio in the reaction cell is calculated by:

$$X_{\text{syr rxncell}} = \frac{F_{std} * c * F_{syr} * \frac{22.4}{F_{std}} * F_{sample}}{F_{excess} + F_{sample}} \Big/ F_{CIMS} \quad (2)$$

where c is the aqueous concentration of the standard within the syringe (M), F_{syr} is the syringe aqueous flow rate (L min^{-1}), 22.4 (L $mole^{-1}$) is a conversion factor for standard liters of gas per mole of substance at STP (273.15 K and 1013.25 hPa), F_{std} is the mass flow rate of the standard carrier gas, F_{excess} is the inlet excess (slpm) removed from the CIMS to increase the sample size (Section 2.1), and F_{CIMS} and F_{sample} are the same as above.

The peroxide and organic acid sensitivity factors are impacted by the inlet pressure because changing the pressure affects the sample flow (F_{sample}), the inlet excess flow (F_{excess}), and the reagent N_2 flow (F_{N2}). As ambient pressure decreases the sample and excess flow rates decrease and F_{N2} increases.

Table 2 shows the calculated sensitivity factors used for both organic acids with respect to the inlet pressure for the three calibration systems: coil, one-syringe, and two-syringe. As discussed above, only the FRAPPE aqueous standards were standardized against a primary reference material. There is a small percent error so it is assumed that both laboratory and FRAPPE standards are accurate to three significant figures.

The water vapor mixing ratio in the reaction cell is used to develop sensitivity factors as a function of specific humidity. It was calculated assuming water equilibration in the humidified line at the set point temperature of the coil water bath (normally 288 K and occasionally 298 K; see above):

$$X_{\text{water rxncell}} = \left(\frac{P_{\text{sat,288K}}}{P_{1013}}\right) * \left(\frac{F_{H_2O}}{F_{\text{Aadco}}}\right) * \left(\frac{F_{\text{sample}}}{F_{\text{CIMS}}}\right) \quad (3)$$

where P_{sat} (hPa) is the water saturation pressure at 288 K (or 298 K), F_{H2O} is the air flow rate (slpm) through the humidified line and P_{1013}, F_{Aadco}, F_{sample}, and F_{CIMS} are the same as above.

All of the sensitivities (cts/ppb) reported here are corrected for the aging of the ion source. Polonium-210 has a half-life of 138 days and as the ion source decays there is a decrease in signal response. The signal response needs to be corrected so that experiments from different points in time can be compared regardless of the age of the ion source. This correction treats the signal response as measured with a new ion source. In the field, new ion sources are used because of licensing and shipping constraints. In the laboratory, the polonium source is replaced annually because of decrease in activity and licensing agreements. The correction factor is the fraction of the actual signal response (N) to the signal response from a new ion source (N_0) in the radioactive decay equation ($N/N_0 = \exp(-t\lambda)$). The correction factor was applied to the experiments if the ion source had decayed at least 25%

All organic acid data reported here are for the HFo and HAc iodide clusters at 173 (I^-•HCOOH) and 187 (I^-•CH_3COOH) townsend, respectively. Any laboratory sensitivities (cts/ppb) reported are blank subtracted.

3. RESULTS

The following results establish the calibration process used to quantify the DC3 organic acids. The coil and one-syringe microfluidic work was with the “Le Breton” iodomethane regent gas mixture (Section 3.1). After previous work with HP and MHP

found that sensitivity is water and pressure dependent, organic acid work with the Le Breton mixture was used to check the published method. There was a pressure dependency for both organic acids for the one-syringe calibration system though it was not the same relationship as with the diluted Le Breton mixture. The diluted Le Breton iodomethane mixture (Section 3.2) was prepared because the original mixture was too concentrated to accurately tune to DC3. The water and pressure dependencies were explored in greater detail for this diluted mixture and laboratory fits were derived for both organic acids (Section 3.3). HFo was fit as a function of water and pressure and HAc was fit with a constant value. The laboratory calibration technique (of altering water vapor and inlet pressure) was verified by comparing laboratory and FRAPPE sensitivities (Section 3.4). HFo laboratory calibrations were a factor of two greater than FRAPPE. HAc had good agreement between laboratory and FRAPPE as did the HP and MHP oxygen clusters though they are not reported here. The diluted Le Breton mixture was assessed at five different flow rates to find a balance between I^- and O_2^- ion clusters. Different iodomethane flow rates were also tested to find the most appropriate iodomethane mixing ratio for DC3. Laboratory calibrations for the HP iodide cluster were compared to DC3 HP calibrations (Section 3.5) to determine the appropriate iodide flow rate. Finally, the study regions for DC3 are described and vertical profiles for both organic acids in each region are presented (Section 3.6).

3.1 Le Breton Mixture

The laboratory calibration sensitivities for the coil (open circles) and a one-syringe microfluidic standard addition system (dots) were compared as a function of reaction cell water vapor for HFo and HAc. The results are shown in Figures 6 and 7,

respectively. In this comparison, the 0.33% iodomethane reagent gas mixture (the "Le Breton" mixture) was used. The organic acid sensitivities at five different inlet pressures were determined (120, 180, 360, 600, and 1013 hPa) and these are identified in Figures 6 and 7 as well. Only experiments at the two highest pressures (600 and 1013 hPa**)** were conducted using the coil calibration system. The laboratory coil sensitivities are a factor of two to three greater than the microfluidic sensitivities for HFo and comparable for HAc using the Johnson et al. (1996) Henry's Law constants. The error bars represent one standard deviations and the calculations are described in Appendix A. There is a pressure dependency for both organic acids. The highest sensitivity for both acids was at the lower inlet pressures (120, 180, and 360 hPa). The pressure dependency is greater for HAc. Since this iodomethane mixing ratio was not used for field calibrations this pressure dependency was not explored further. Both the coil and microfluidic HFo sensitivities increase as the water mixing ratio increases. The microfluidic HAc measurements show no trend with water in the sampled range identifiable outside of the daily signal noise. The coil HAc measurements decrease above a water mixing ratio of 2000 ppm.

A wide range of Henry's Law constants ranging from 5.43 to 13.2 M/hPa and 5.43 to 9.18 M/hPa have been reported for HFo and HAc at 298.15 K, respectively (Sander 1999). The coil and microfluidic laboratory calibration systems compare the best with the Johnson et al. (1996) Henry's Law constants. Laboratory derived Henry's Law constants were calculated as well (Table 3). The laboratory calculated Henry's Law constants for HAc are similar to the Johnson et al. (1996) values. This indicates that Johnson et al. (1996) accurately quantified the HAc gas-phase

partitioning. The laboratory calculated Henry's Law constants for HFo are lower than the Johnson et al. (1996) values. The difference in Henry's Law constants could be due to a higher gas-phase partitioning through the coil system than measured by Johnson et al. (1996). Therefore, the HFo mixing ratio in the reaction cell is greater than expected which results in an overestimation of the sensitivity of the CIMS towards HFo. This overestimation explains the difference between the coil and microfluidic system.

For both the coil and one-syringe microfluidic calibration systems, there is an overall increase in HFo sensitivity throughout the water vapor range examined. At the higher water mixing ratios the HFo sensitivity begins to plateau. The lower pressure work has a linear relationship because only low water vapor mixing ratios are possible. The HAc water vapor dependence is insignificant and within the daily variance for the various pressure runs. The HAc coil sensitivity decreases above a water mixing ratio of 2000 ppm. For the purpose of this work, the HAc and water relationship with the Le Breton iodomethane mixture is treated as negligible.

3.2 Diluted Le Breton Mixture

Peroxides and organic acids were calibrated together with the two-syringe microfluidic calibration set-up described in Section 2.3. Five different iodomethane flow rates (0.0005 to 0.0025 slpm) were assessed with the second iodomethane mixture (5 ppm in N_2) for the blended CH_3I and $CO_2 \bullet O_2^-$ reagent gas. The CIMS precision and accuracy were calculated using laboratory work at the 0.0005 slpm iodide flow rate because this was used for FRAPPE and DC3. The HFo and HAc precision (1 standard deviation of the blank signal response) are 15.4 and 15.0 ppt,

respectively. It is outside of the scope of this work to determine inflight precision. The instrumental accuracy was estimated using calibration precision and is 23.3% and 25.0% accurate for HFo and HAc, respectively.

The amount of iodide present in the CIMS was monitored with the iodide and water cluster ($I^-•H_2{}^{18}O$) at 147 townsend (Figure 8). This cluster provided a quick response as the water and iodomethane were altered. The HFo and HAc sensitivities as a function of the reaction cell water mixing ratio along with the standard deviations are in Figures 9 and 10, respectively. The same inlet pressure work as above was performed for each iodomethane flow rate. The individual pressures are not listed to simplify the figures.

As with the Le Breton calibration work above, the HFo sensitivity increased as a function of water and there is no trend for HAc outside of the instrumental variance. The lowest HFo and HAc sensitivities are at 1013 hPa which is unexpected because the most water and I^- is present in the reaction cell at ambient pressure. As a result, it was hypothesized that the highest sensitivity (especially for HFo) would be at ambient pressure. Since this was not the case, the dynamics between iodomethane, pressure, and water for both acids were investigated.

The impact of iodomethane on sensitivity was examined using the maximum sensitivity at each inlet pressure for both acids as a function of the iodomethane flow rate. This is illustrated in Figures 11 and 12 for HFo and HAc, respectively. Both acids are fit with a linear and quadratic fit and 95% confidence intervals. Three outlier points for HFo at 600 hPA were removed from the data set as they fell well outside the 95% confidence interval for both fits. One day of HAc work at 1013 hPa was

markedly below the rest of the work at that pressure so that day was removed as well from any subsequent work. While it is possible that this low day is due to human error, there is not a similar decrease in sensitivity for HFo or the peroxides. Visually both fits represent the data (with the exception of 600 hPa for HFo) so the F-test was used to determine the best fit. It was found that there is no significant difference between the fits for both acids at all the pressures within the tested flow rate range. The sixth panel in Figures 11 and 12 show maximum sensitivity regardless of pressure as a function of iodomethane flow rate. The standard deviation bars represent the impact of pressure on sensitivity. The sensitivity for both organic acids tripled from the lowest (0.0005 slpm) to the highest (0.0025 slpm) iodomethane flow rate.

3.3 Water and Pressure Dependencies and Calibration Fits

Water and pressure dependencies were studied using the ratio of the sensitivity to the maximum sensitivity. Only the work at the 0.0005 slpm iodomethane flow rate is reported. This ratio removed the bias of daily variation in the instrument. An average of this sensitivity ratio for each water vapor value was used to combine the different experimental days. These ratios as a function of the reaction cell water vapor are shown in Figures 13 and 14 for HFo and HAc, respectively. The sixth panel shows all the pressures together as a function of the water mixing ratio. For each pressure, the maximum sensitivity (ratio of one) for HFo was at the highest water vapor mixing ratio. The HAc maximum sensitivity was not at the same water mixing ratio for the different pressures or between days. This is why the ratio is always less than one. The lowest HAc sensitivity was always within 50% of the maximum sensitivity regardless

of pressure. This supports what was seen above that the HAc-water relationship is small and not a critical determining factor to the sensitivity.

These ratios were not sufficient to study pressure dependencies. The sensitivities at each pressure were calculated using the sensitivity ratios and the averaged maximum sensitivity for each pressure. This calculated sensitivity will be referred to as the "cleaned-up sensitivity". The cleaned-up sensitivities were calculated for each iodomethane flow rate though only the sensitivities at 0.0005 slpm are reported. The cleaned-up sensitivities (and one standard deviation) for HFo at each pressure as a function of the reaction cell water vapor are in Figure 15. Even with the cleaned-up sensitivity there is still a noticeable difference between the pressures as seen in the sixth panel. Therefore the HFo fit must be a function of water and pressure. The HFo sensitivity initially increases with water vapor and reaches an asymptote at the highest water mixing ratios – especially at higher pressure which also has the largest water mixing ratio. A Michaelis-Menten fit

$$y = \frac{Ax}{B+x} + C \tag{4}$$

is used to represent this increase and subsequent plateau in sensitivity at higher water. The water dependency coefficients for HFo also change as a function of pressure. As mentioned above the highest pressure (1013 hPa) sensitivity was unexpectedly low. Therefore, the three coefficients were determined without 1013 hPa. The equations for the three coefficients are

$$A = \exp\left(\left(\frac{-6.5\times10^{6}}{P^{3}}\right) + \left(\frac{2.7\times10^{5}}{P^{2}}\right) + \left(\frac{-1.0\times10^{3}}{P}\right) + 11.0\right)$$
$$B = \exp\left(\left(\frac{2.1\times10^{5}}{P^{2}}\right) + \left(\frac{-9.7\times10^{2}}{P}\right) + 9.02\right) \tag{5}$$

$$C = \exp(-6.2\text{x}10^{-6}P^2+4.6\text{x}10^{-3}P+7.4)$$

where P (hPa) is pressure. The pressure and water fit (Figure 15 – black line) represents the data well with the exception of 1013 hPa which is overestimated when compared to the water fit (Figure 15 – green line). The calculated pressure fit values (A, B, and C) are higher than the measured work for 1013 hPa. The fit without 1013 hPa is used for HFo from this point forward. The cleaned-up sensitivities (and one standard deviation) for HAc as a function of reaction cell water vapor for each pressure along with the water fit (green line) are in Figure 16. The sixth panel shows all the pressures together as a function of reaction cell water vapor. There is a pressure dependency; however, the difference in sensitivities for the pressures is small. Several different fits as a function of water and/or pressure were considered but none of them accurately reproduced the laboratory or field sensitivities or contributed enough explanation of variance to warrant additional fitting terms. It was decided to use an average constant value (752.5 cts/ppb) for HAc sensitivity. The laboratory data and fits are compared to field data to confirm the accuracy of the fits.

3.4 FRAPPE Organic Acid Calibrations

In-flight calibrations from FRAPPE are compared to the cleaned-up laboratory sensitivities for HFo and HAc (Figures 17 and 18). The laboratory data are the same as Figures 9 and 10. Both laboratory and FRAPPE calibrations used the second CH_3I mixture (5 ppm, 0.0005 slpm) and CO_2•O_2 (400 ppm CO_2, 0.080 slpm) as the blended reagent gas with the two-syringe microfluidic calibration set-up. The laboratory sensitivities (blue squares) were corrected for the aging ^{210}Po ionization source. The HFo laboratory calibrations are a factor of two higher than the in-flight calibrations

with the 1013 hPa calibrations closest to the in-flight calibrations. Even though the laboratory calibrations are higher the trend is the same. Both the FRAPPE and laboratory sensitivities increase as a function of reaction cell water vapor. The low water laboratory calibrations are when the system is "dry" and the only water comes from the syringe addition. The lowest in-flight calibrations were during RF04. The HAc calibrations align between laboratory and field measurements with a few exceptions. All in-flight calibrations from RF04 and one from RF11, all with similar water mixing ratios, are significantly lower than the rest of the in-flight calibrations. The laboratory fits were tested using the FRAPPE calibration data and reasonably represented the in-flight calibrations.

3.5 DC3 Hydrogen Peroxide Calibrations

The final calibration step was to determine which iodomethane flow rate of the 5 ppm in N_2 mixture best represented DC3 conditions. This was done using HP because it clusters with iodide and was calibrated for during DC3. The laboratory sensitivity for the HP and iodide cluster at 161 townsend ($I^-•H_2O_2$) as a function of reaction cell water vapor is in Figure 19 for the five different iodomethane flow rates. As expected, the HP sensitivity increases as the proportion of iodomethane in the reaction cell increases. The different iodomethane flow rates were compared to DC3 in-flight calibrations though they are not all shown here. The 0.0005 slpm iodomethane laboratory calibrations (blue squares) for $I^-•H_2O_2$ correspond well with the DC3 in-flight calibrations (Figure 20). Therefore the laboratory derived fits for HFo and HAc using the 0.0005 slpm iodomethane flow rate will be used to quantify both organic acids during DC3.

3.6 DC3 Study Regions and Organic Acid Vertical Profiles

DC3 focused on the chemical and meteorological properties of deep convective systems in three regions. The NCAR GV flight tracks for all flights are in Figure 21 and divided into three study regions indicated by colored boxes: Colorado (red), Oklahoma-Texas (magenta), and the eastern states from Arkansas to the Carolinas (green). All in-flight data for hydroperoxides (HP and MHP) and organic acids (HFo and HAc) are in Figures 22, 23, and 24 for the three study regions as a function of altitude. The symbols are the median values, the thicker lines are the interquartile range, and the thin lines are the 10^{th} and 90^{th} percentile range. Any stratospherically influenced air is removed by filtering out high ozone (greater than 150 ppb) and low carbon monoxide (less than 70 ppb). There is a decrease in HP throughout the altitude profile for all three study regions. There is a decrease in MHP for the bottom 6 km and then a small increase at higher altitudes due to deep convection. All three study regions show deep convective transport at high altitudes based on the enhancement of MHP relative to HP.

Each study region has higher HAc mixing ratios compared to HFo. In general, all three profiles have a decrease in HFo up to 6 km followed by an increase either back to boundary layer mixing ratio values or higher (a so called "C" shape). This profile is most pronounced in the Eastern region. The Eastern region also has the highest altitude measurements and the HFo sensitivity starts to decrease again above 12 km. The highest mixing ratios of both organic acids in the Oklahoma-Texas region were measured at 2 km. The Colorado HFo profile has more HFo at the top of the profile than in the boundary layer. The HAc altitude trend is not as strong in any of the

study regions though the mixing ratio decreases up to 6 km. The Eastern region has the biggest difference between both acids at high altitude. The largest range of mixing ratios (represented by the 10^{th}-90^{th} percentile) is in the Oklahoma-Texas region and is reflected in the peroxide and organic acid profiles.

4. DISCUSSION

4.1 Ionization Chemistry and Water Sensitivity Dependence

Jones et al. (2014), Le Breton et al. (2012), and Lee et al. (2014) have observed a HFo sensitivity dependence on water vapor. Lee et al. (2014) has shown HAc sensitivity to vary with water vapor. HFo and HAc sensitivities were examined over a range of water vapor mixing ratios from a few ppm to 20,000 ppm with a combination of laboratory and field measurements.

The following ion chemistry is invoked to account for HFo's observed sensitivity dependence on water vapor.

$$I^- + HCOOH \rightarrow I^-\bullet HCOOH$$

$$I^- + H_2O \rightarrow I^-\bullet H_2O$$

$$I^-\bullet H_2O + HCOOH \rightarrow I^-\bullet HCOOH + H_2O$$

$$I^-\bullet HCOOH + H_2O \rightarrow I^-\bullet H_2O + HCOOH$$

With the addition of a little water, the reaction to form $I^-\bullet HCOOH$ occurs faster than to $I^-\bullet H_2O$ from an $I^-\bullet HCOOH\bullet H_2O$ intermediate cluster (Lee et al, 2014). Lee et al (2014) found the sensitivity plateaus and declines when the reaction cell water was above 2200 ppm. Unlike Lee et al. (2014), our HFo sensitivity did not decrease towards the higher water mixing ratios though it did plateau - especially the ambient pressure work (1013 hPa). The water mixing ratio in the reaction cell could not be increased enough

to achieve a decline in sensitivity. The maximum water mixing ratio in the reaction cell during laboratory experiments was 7800 ppm. The FRAPPE in-flight calibrations covered a larger water mixing ratio yet there was still no decline in sensitivity. It is likely that variations in the CIMS configurations cause the differences in response as a function of water. Lee et al. (2014) used a permeation tube and not a gaseous mixture to add the iodide. It is possible that a difference in the total amount of iodide available impacts clustering preference. Their standard addition system differed from ours as well as they had no water present in their driest conditions. We never had a completely dry system as the standards were prepared in aqueous solutions. Lee et al. (2014) also had a higher reaction cell pressure (90 hPa) which could impact reaction cell chemistry. Le Breton et al. (2012) did not discuss a decrease in sensitivity as a function of water but they did note that water was needed to promote clustering. They added water to the reagent gas to ensure ion clustering. Jones et al (2014) found a decrease in sensitivity at the lowest water mixing ratios as a result of an insufficient water source to promote clustering. Both Le Breton et al. (2012) and Jones et al. (2014) used similar reaction cell pressures (~22 hPa) to our work. Even though all these systems use iodomethane for HFo clustering the differences reflect the impact instrumental modifications can have. This is why it is important for each CIMS to be calibrated extensively for all target species.

Lee et al (2014) found a decrease in HAc sensitivity with the addition of any water to the system. Using Lee et al. (2014) as a guide our HAc sensitivity should obey the following reaction sequence.

$$I^- + M + CH_3COOH \rightarrow I^- \bullet CH_3COOH + M$$

$$I^- \bullet CH_3COOH + H_2O \rightarrow I^- \bullet H_2O + CH_3COOH$$

However, we found no significant decrease in sensitivity in this CIMS configuration as a function of water in either the laboratory or during FRAPPE. The HAc sensitivity is low and there is no appreciable water relationship outside of instrumental variance. There is minimal other literature data available for the HAc and iodide cluster. Acetate is a commonly used reagent gas for CIMS systems; therefore, HAc is not detected. HAc has been measured using proton transfer reaction mass spectroscopy (PTR-MS) and HAc sensitivity decreased with the addition of water (Baasandorj et al. 2014). Unfortunately, a direct comparison is not possible as this a different instrumental set-up and reagent chemistry.

4.2 Ionization Chemistry and Iodide Concentration Dependence

The goal of the dual reagent gas system was to monitor HP, MHP, HFo, and HAc. This requires a balance between the iodide and oxygen chemistry. In general, as the proportion of iodomethane increases the sensitivity of the CO_2 and O_2 clusters decreases. The negative impact on sensitivity is greater for MHP than HP as discussed earlier. MHP is an important target species and it is critical to find a reagent ion balance that does not reduce the sensitivity significantly. This CIMS is not as sensitive to HAc as HFo thus a decrease in iodide results in a larger reduction of HAc sensitivity. Finding a balance between the two reagent gases ultimately depends on a balance between MHP and HAc. The lowest iodomethane flow rate was chosen for FRAPPE as there was a quantifiable HAc addition with a minimal impact on MHP. Based on the HP and iodide cluster (at 161 townsend) this iodomethane flow rate also represents the iodide mixing ratio during DC3. It was fortuitous that there was enough

iodide present during DC3 to promote organic acid clustering without significantly impairing the MHP sensitivity.

4.3 Ionization Chemistry and Pressure Dependency

It was originally thought that the HFo maximum sensitivity would be at the highest pressure since that is the highest water mixing ratio and HFo sensitivity increases as a function of water. However, the highest pressure actually had the lowest sensitivity for both organic acids. At the 0.0005 slpm iodomethane flow rate, the maximum sensitivities for HFo and HAc were at 600 and 360 hPa, respectively. Unfortunately, at this time it is not possible to fully understand the underlying cause. Pressure dependency will not be an issue for future work with this CIMS as a variable orifice will be added that maintains constant sample and reagent gas flow rates. It is possible that this pressure dependency is a function of the iodide-oxygen relationship in the reaction cell. As discussed above, the addition of iodide results in a decrease in sensitivity of the oxygen dependent clusters (i.e. MHP). However, it had not been explored that the oxygen could negativity impact the iodide clusters. A chemical computational diagnosis to test the strength of the ion clusters is not accessible at this time. This limits the extent to which this problem can be investigated. Even though this situation will be resolved for future field work it still needs to be explored for past missions. A potential reason for the unexpected pressure relationship is discussed here.

The ratio of iodide to oxygen through the ion source is constant regardless of the inlet pressure because the only source of oxygen is from the $CO_2 \bullet O_2$ reagent gas. The iodide to oxygen ratio varies inside the reaction cell due to the oxygen in the sample flow. The changing sample flow rate results in a dilution of iodide with respect

to oxygen as pressure is increased. Therefore, if there is a negative impact on the iodide chemistry it would be at the greatest sample flow rate (1013 hPa) as this represents the greatest oxygen addition to the system which is seen for both organic acids. However, if this was a linear relationship then the greatest sensitivity should be at 120 hPa. As this was not the case it is likely that there is a threshold for the iodide sensitivity and not a linear dilution factor. It is possible that at 600 hPa HFo is still able to efficiently cluster with iodide though greater than 600 hPa the proportion of oxygen becomes too large to support iodide clustering. As mentioned above, the CIMS is not as sensitive to HAc which could explain why the maximum sensitivity is at an even lower inlet pressure (360 hPa) than HFo. Therefore, the original thought process that the highest sample flow rate would result in the highest HFo sensitivity is flawed. Using calibration fits as a function of inlet pressure eliminates the need to fully comprehend the mechanism of the iodide loss in sensitivity. The HFo sensitivities showed the greatest dependency on inlet pressure and are fit as a function of water and pressure. HAc also had a pressure dependency though the addition of a pressure dependency term does not add significant improvement to the HAc fit and is not used.

4.4 Ethanol Interference

Concentrated ethanol responds at 173 townsend ($I^-•C_2H_6OH$) and can be used as a CIMS system leak check. The CIMS sensitivity towards ethanol was tested to confirm that ethanol could serve as a leak check without significant ambient signal interference. Ethanol was added via the 2-syringe microfluidic and coil standard addition systems. The microfluidic standard (~ 6mM) was prepared to be equivalent to

HFo standard during FRAPPE. The coil standard (0.2 mM) was prepared at a similar concentration to MHP due to the similarities in the Henry's law constant. The Henry's Law constant (0.20 M/hPa) used for the coil system was from Sander (1999) and is temperature independent. Similar to HFo, ethanol's sensitivity increased with the addition of water though ethanol's sensitivity was significantly lower than HFo at both the minimum (100x lower) and maximum (30x lower) water concentrations used in the laboratory. Baasandorj et al (2014) performed similar work with a PTR-MS and found HFo's sensitivity to be 5-20x higher than ethanol. We strongly recommend verifying that the ethanol measured in the study region is low (background mixing ratios).

4.5 DC3 Case Study: Research Flight 03

The DC8 and GV sampled convection in the Alabama radar region during Research Flight 3 (RF 03) on May 21, 2012 and the flight tracks for both aircraft are in Figure 25. The GV sampled convective outflow at several altitudes along the Alabama-Tennessee border (19:00 to 20:45 UTC) and then executed a spiral descent to 0.9 km before returning back to base. HFo and HAc measurements as a function of time and altitude are in Figure 25. The altitude (m) is also given as a function of time for reference. The maximum HFo and HAc mixing ratios were 720 ppt and 1900 ppt, respectively. The largest HFo mixing ratios were between 8 and 10 km during the storm sampling with the peak at 8.6 km. The largest HAc mixing ratios sampled were at the lowest altitude. The ratio of HFo to HAc is less than one for the majority of the flight reflecting the substantial HAc sampled regardless of altitude. Higher HAc

relative to HFo was measured during the whole campaign in each of the study regions (Figures 22, 23 and 24).

Previous field measurements have reported varied results about the proportion of HFo to HAc. Reiner et al. (1999) and Talbot et al. (1996) reported greater HAc relative to HFo (up to twice as much HAc as HFo). Millet et al. (2015) sampled HFo and HAc during the summer over the US Southeast. Millet et al.'s HFo mixing ratios are an order of magnitude higher than reported here though HAc mixing ratios are within Millet et al.'s standard deviation. Millet et al. sampled during warm, sunny days (June and July) which is conductive to HFo formation. Deep convective storms were the priority for DC3 (May and June) which leads to a preferential sampling of cloudy, damp days. The high solubility of HFo and the large extent of vertical mixing characteristic of these storms likely led to a preferential sampling of conditions that would dilute, and possibly remove, HFo.

The altitude profile for HFo has a "C" shape with higher mixing ratios near the surface and at high altitude (above 6 km). HAc follows a similar trend with a weaker gradient. For the majority of flights during DC3 there is little change for HAc as a function of altitude. The eastern region flights, especially RF 03, have the most pronounced "C" shape. The majority of available literature data for HFo and HAc do not sample the full DC3 altitude range (0 – 13 km). Millet et al. (2015), Reiner et al. (1999), and Talbot et al. (1996) all report a decrease in HFo with altitude though only Reiner et al. and Talbot et al. sampled above 7 km. The location and time of year will also impact the organic acid mixing ratios and altitude profiles. Tablot et al. and Reiner et al. both sampled in different global regions and at a different time of year

(fall). Considering the diverse sources for both acids and the *in situ* gas-aqueous phase dynamics it is not surprising that this pattern is not seen consistently.

The Alabama-Tennessee border region is dominated by biogenic and anthropogenic emissions especially from Birmingham (Barth et al. 2014). The HFo measured between 8 and 10 km was higher than in the boundary layer. This could be the result of *in situ* photochemical production from biogenic precursors. Most reported chemical tracers do not show a similar elevation between 8 to 10 km with the exception of methanol. Methanol is a biogenic tracer and was measured by the Trace Organic Air Analyzer (TOGA, NCAR) onboard the GV. The methanol mixing ratio as a function of altitude is in Figure 26. Millet et al. (2015) found the strongest correlation between methanol and HFo which supports the importance of biogenic sources in this region. There is minimal data available for other biogenic tracers during RF 03 though moderate isoprene (600 ppt), a known HFo precursor, was sampled during the lower altitude leg over Tennessee. The elevated HFo was measured in a storm outflow as indicated by the increase of MHP relative to HP (Figure 25). Therefore it is possible that this increase in HFo is the result of *in situ* photochemistry from biogenic precursors lofted up.

A large portion of the flight was at high altitude which can be impacted by stratospheric air masses. The chemical composition of the stratosphere is different and this will impact the chemical dynamics. The high ozone in the stratosphere could result in an ozone artifact in the CIMS measures at 80 townsend ($O_3 \bullet O_2$). The two stratospherically influenced air masses (identified by high ozone and low carbon monoxide) are removed.

Convection in Alabama was the weakest of the three study regions (Barth et al. 2014). Convective outflow is characterized by a relative increase of MHP to HP. Convective transport is identified above 8 km with the strongest outflow above 10 km. This is confirmed by Barth et al. (2014) using other soluble and boundary layer tracers in conjunction with peroxides. There is an enhancement of HAc relative to HFo at the highest altitude (above 10 km) during RF 03 though at this time it is not enough evidence that organic acids can be used as convective transport tracers. Peroxides are a more reliable convective transport tracer because there is a clear reversal in the relationship between the two from the surface (HP>MHP) to the storm outflow (MHP>HP). The solubilities of organic acids are more complicated due to the pH dependency and thus not as reliable of a tracer. HFo and HAc could be used as a secondary tracer especially in a biogenically dominated region. Using organic acids as convective transport tracers needs to be investigated further.

There was a descent to 0.9 km towards the end of the flight over Tennessee. There was an increase in HFo and the highest measured HAc for this flight. As mentioned above, Tennessee is known for high biogenic emissions. An air quality cancer study in Tennessee found elevated levels of acetaldehyde in the summer primarily as the result of secondary formation from biogenic VOCs (Díaz-Robles, Fu, and Reed 2013). The OH oxidation of acetaldehyde forms HAc from the peroxy acetyl radical. Acetaldehyde, also measured with the TOGA, is shown as a function of altitude in Figure 26. Acetaldehyde increased from 100 ppt at 10 km to 800 ppt near the surface. The lower HFo response near the surface could be because HFo was scavenged in the storm. HFo is more soluble than HAc at typical rain pH values.

Unfortunately, there is no low altitude work during the other flights in the region for comparison. There are higher altitude flights in this region that see the elevated HAc relative to HFo though the mixing ratios are higher for RF 03 than the other flights. There were only two days classified as Alabama storm sampling and RF 03 was the stronger case (Barth et al. 2014). The other flight had less than 500 ppt for both acids when sampling in a similar region. It is possible the stronger storm lofted more organic acid precursors than during the other flight. The other difference is that there should be more iodomethane earlier on in the campaign which could result in a difference of sensitivities. However, flights in other regions later in the campaign still saw substantial responses for both acids.

5. CONCLUSIONS

This work successfully replicated Le Breton's iodomethane reagent gas mixture for the measurement of HFo and HAc. Based on microfluidic and coil experiments it was possible to calculate Henry's Law constants for both organic acids which are comparable to literature values. A blended reagent gas mixture (CO_2 in air and CH_3I) was developed and deployed in the field during FRAPPE measuring HP, MHP, HFo, and HAc. Calibration fits using the blended reagent gas were determined for HFo (as a function of inlet pressure and water) and HAc (an average value independent of inlet pressure and water). These calibration fits made it possible to quantify both organic acids measured during DC3. All three DC3 study regions were characterized by greater HAc relative to HFo throughout the altitude profile. Both organic acids had a "C" shaped altitude profile for the majority of the flights. A test

case, RF 03, was highlighted which represents a deep convective storm influenced by biogenic tracers.

TABLES

Table 1: Reagent gas mixing ratios as a function of CH_3I and N_2 mass flow rate

Inlet Pressure (hPa)	1013	600	360	180	120
N_2 Mass Flow Rate (slpm)	2.03	2.99	3.98	4.23	4.27
CO_2 (ppm)	15	10.4	7.9	7.4	7.4
O_2 (ppm)	7512	5212	3941	3712	3678
CH_3I Mass Flow Rate (slpm)	**CH_3I (ppb)**				
0.0005	1.2	0.81	0.62	0.58	0.57
0.0010	2.3	1.6	1.2	1.2	1.1
0.0015	3.5	2.4	1.8	1.7	1.7
0.0020	4.7	3.3	2.5	2.3	2.3
0.0025	5.9	4.1	3.1	2.9	2.9

Table 2: Sensitivity factors for the different calibration systems (coil, 1-syringe, and 2-syringe) for both formic (m/z 173) and acetic (m/z 187) acid

Pressure (hPa)		1013	600	306	180	120
m/z 173	**Coil – 288 K**	0.297	X	X	X	X
	Coil – 298 K	0.603	0.357	X	X	X
	1-Syringe	1.63	1.12	0.749	0.731	0.885
	2- Syringe	1.67	1.20	0.546	0.574	0.780
m/z 187	**Coil – 288 K**	2.07	X	X	X	X
	Coil – 298 K	4.32	2.55	X	X	X
	1-Syringe	1.63	1.12	0.749	0.731	0.885
	2- Syringe	1.67	1.20	0.546	0.574	0.780

Table 3: Comparison of literature and laboratory derived Henry's Law constants for formic and acetic acid

Author	Temperature (K)	Formic Acid (M/hPa)	Acetic Acid (M/hPa)
Johnson, Betterton, and Craig (1996)	288	17.9 ± 2.6	8.42 ± 0.82
Johnson, Betterton, and Craig (1996)	298	8.78 ± 1.3	4.05 ± 0.39
This thesis	288	13.8	7.37
This thesis	298	5.58	4.67

FIGURES

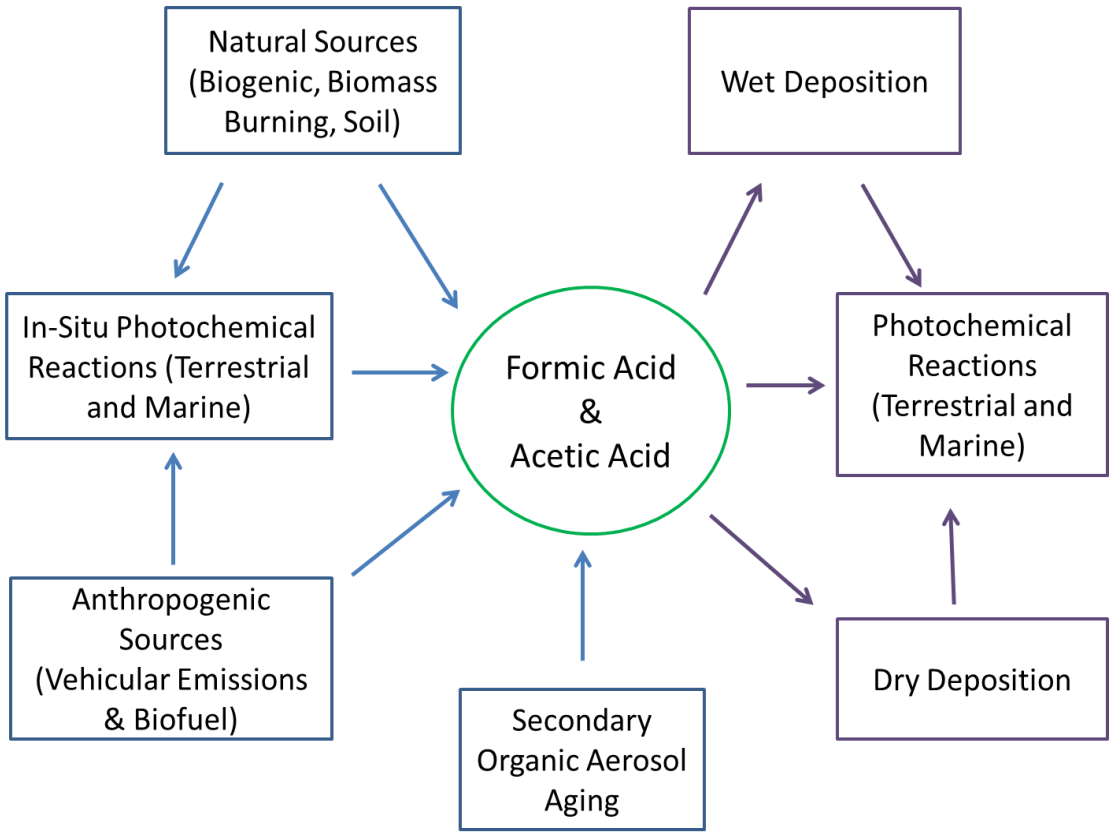

Figure 1: Representation of the biogeochemical cycle for formic and acetic acid with an emphasis on the sources (blue) and sinks (purple).

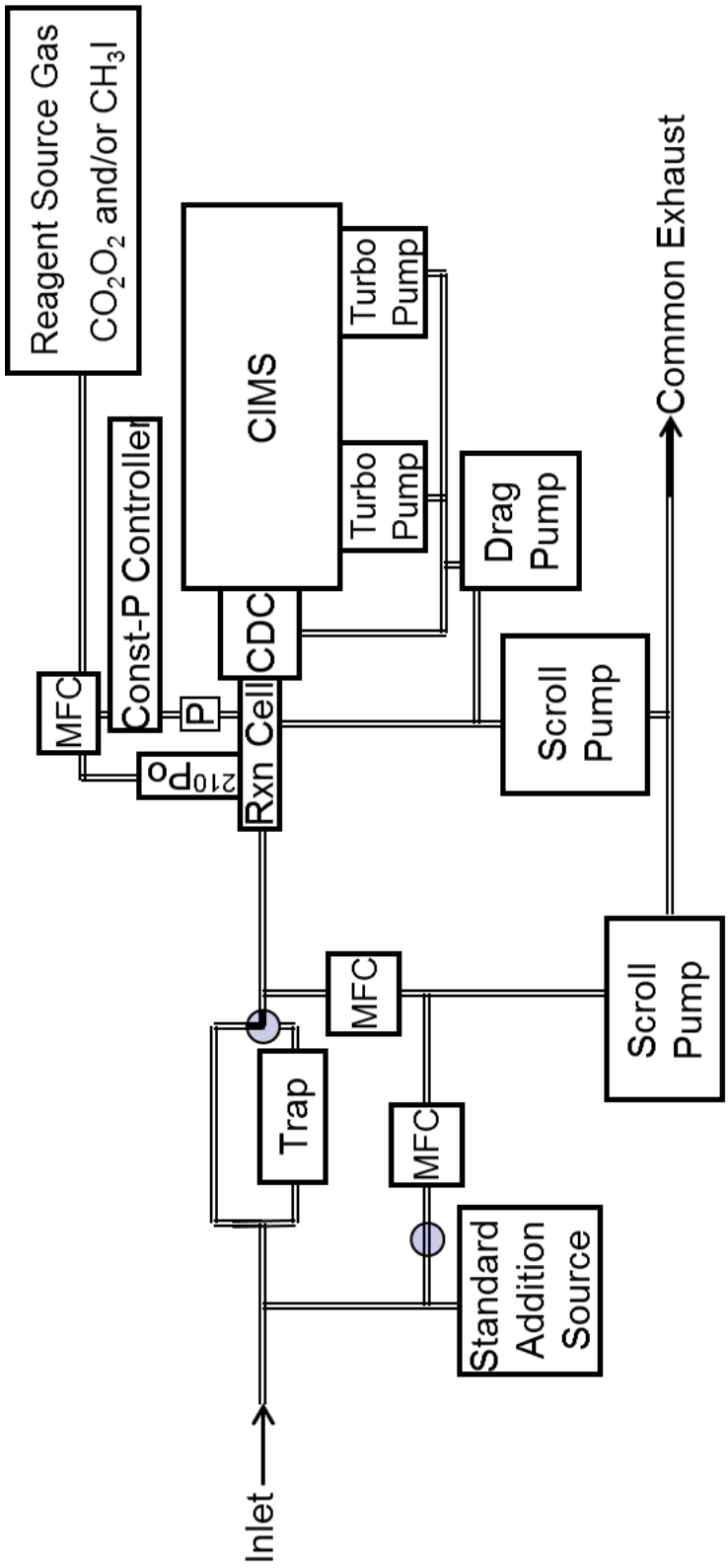

Figure 2: The chemical ionization mass spectrometer (CIMS) instrumental schematic. The air through the inlet is either ambient air or zero air generated from an Aadco (used in the laboratory). CDC refers to the octopole collision dissociation chamber and MFC are mass flow controllers. CIMS represents the quadrupole mass spectrometer

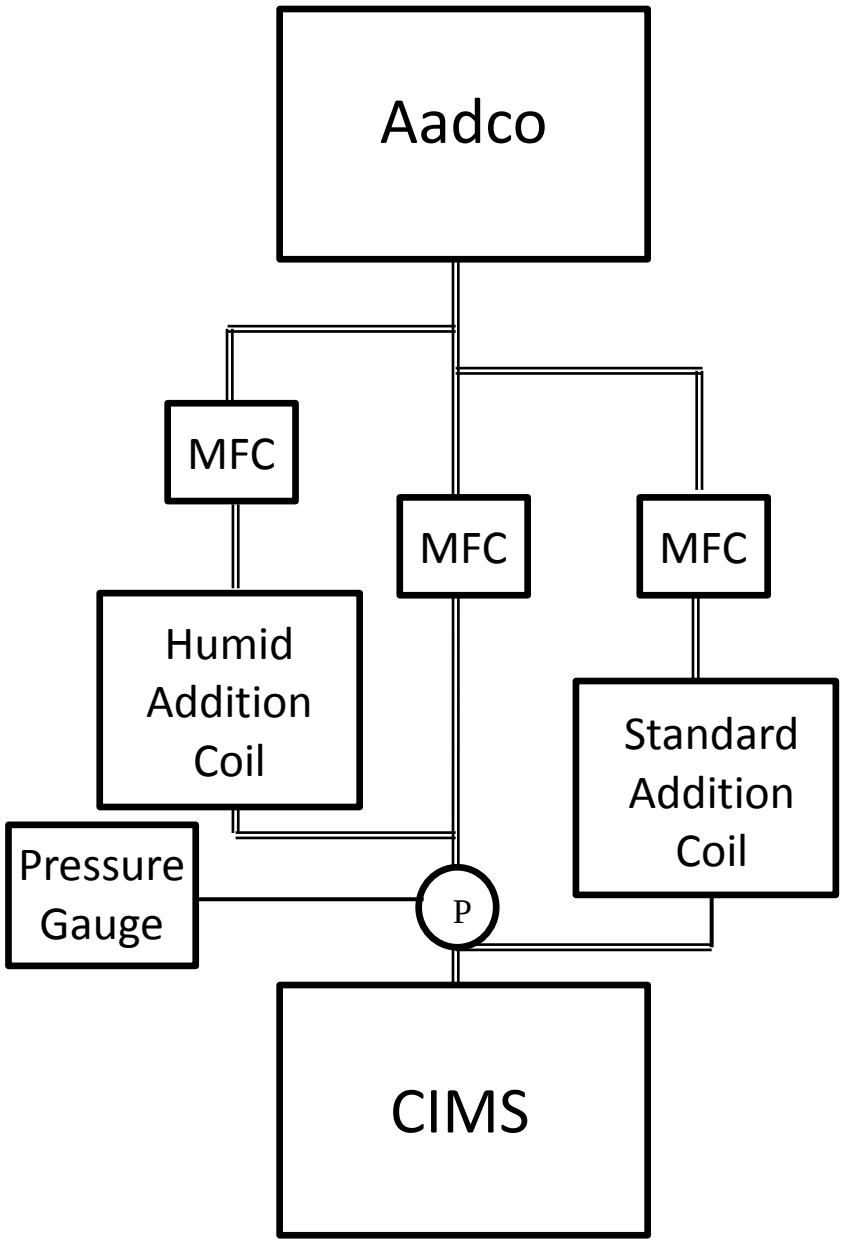

Figure 3: The laboratory schematic for the humidification and inlet pressure experiments. The inlet pressure is controlled by a needle valve (P) and pressure gauge. Detailed layouts for the humidification and coil standard addition systems are found in Figures 4 and 5, respectively. The CIMS box represents the inlet and subsequent instrumental set-up found in Figure 2. All laboratory experiments used the Aadco (zero air generator) as the air source regulated by mass flow controllers (MFC).

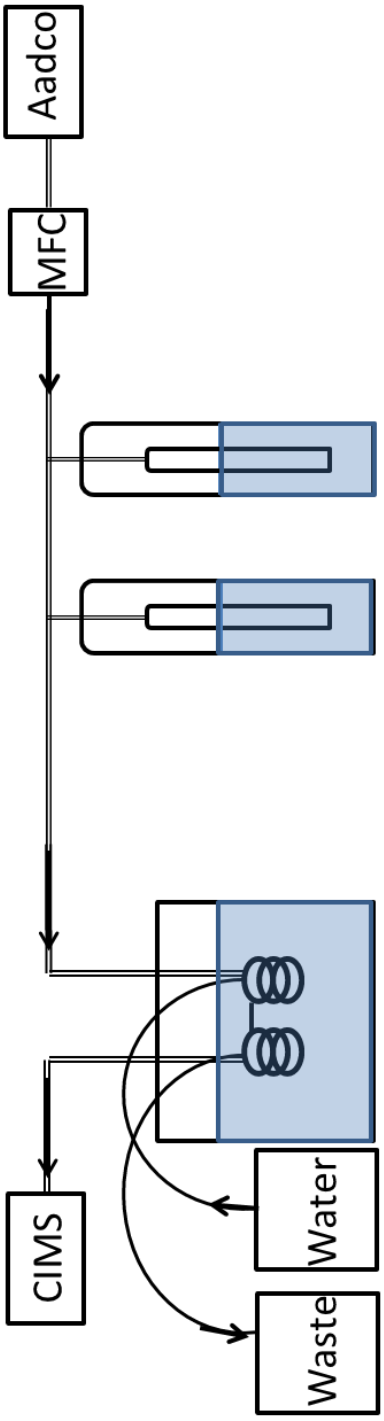

Figure 4: The humidification process set-up used in the laboratory as seen in Figure 3. A fraction of the zero air generated with the Aadco (regulated by a mass flow controller (MFC)) passes through two gas washing bottles increasing the amount of evaporated water in the air stream. The air then passes through a gas-water equilibration coil in a water bath (at 288 or 298 K) allowing control of the water mixing ratio in the air stream before being added back into the main air stream and entering the CIMS.

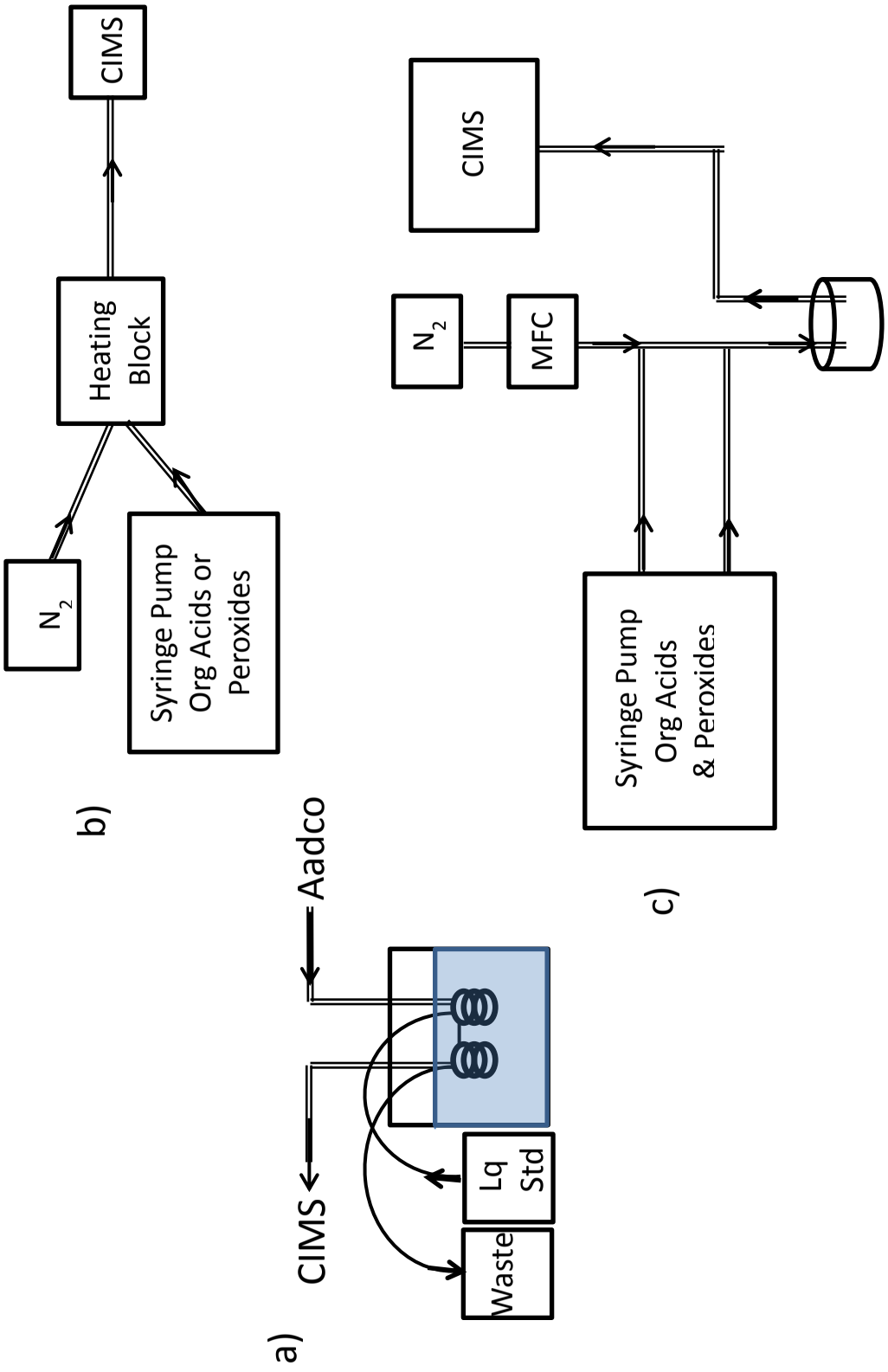

Figure 5: The three laboratory calibration systems described in detail in section 2.3.: a) the coil standard addition system set-up b) the one-syringe microfluidic standard addition system set-up c) the two-syringe microfluidic standard addition system set-up

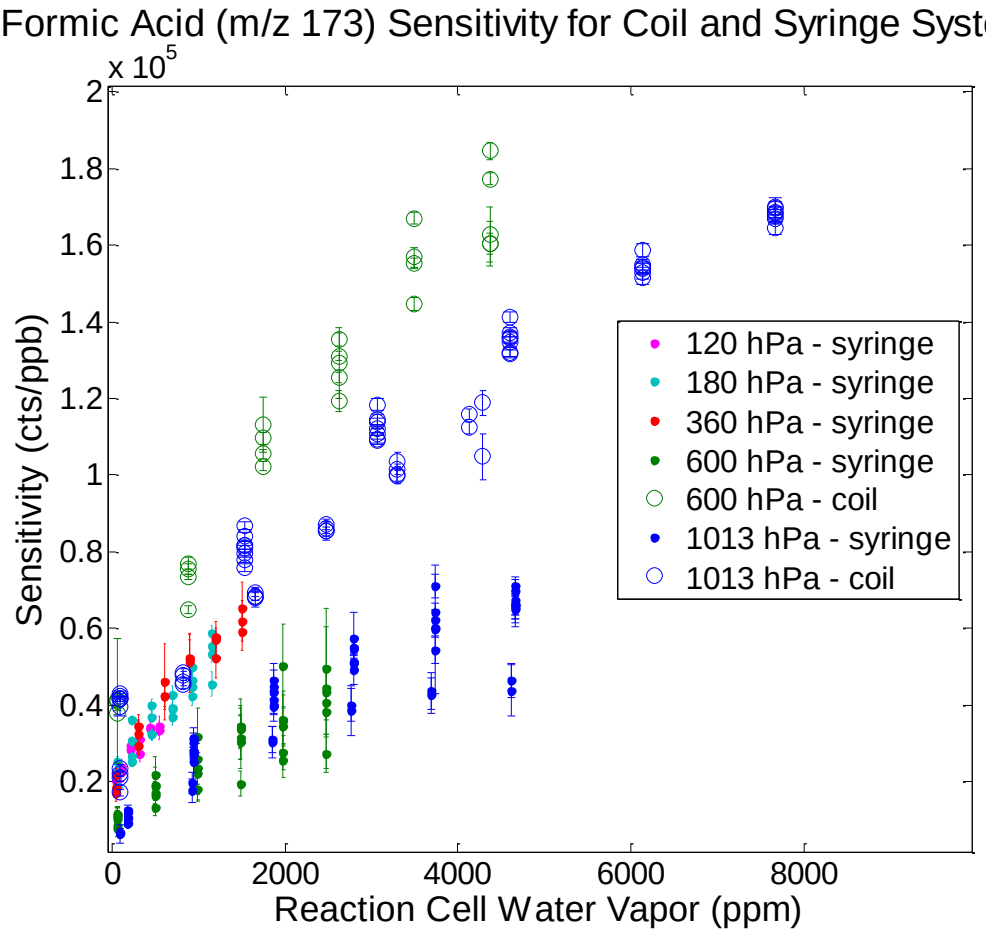

Figure 6: Formic acid sensitivities as a function of reaction cell water vapor for 120, 180, 360, 600, and 1013 hPa for the coil calibration and one-syringe microfluidic calibration systems with the 0.33% iodomethane reagent gas (Le Breton mixture). The bars represent one standard deviation as calculated in Appendix A.

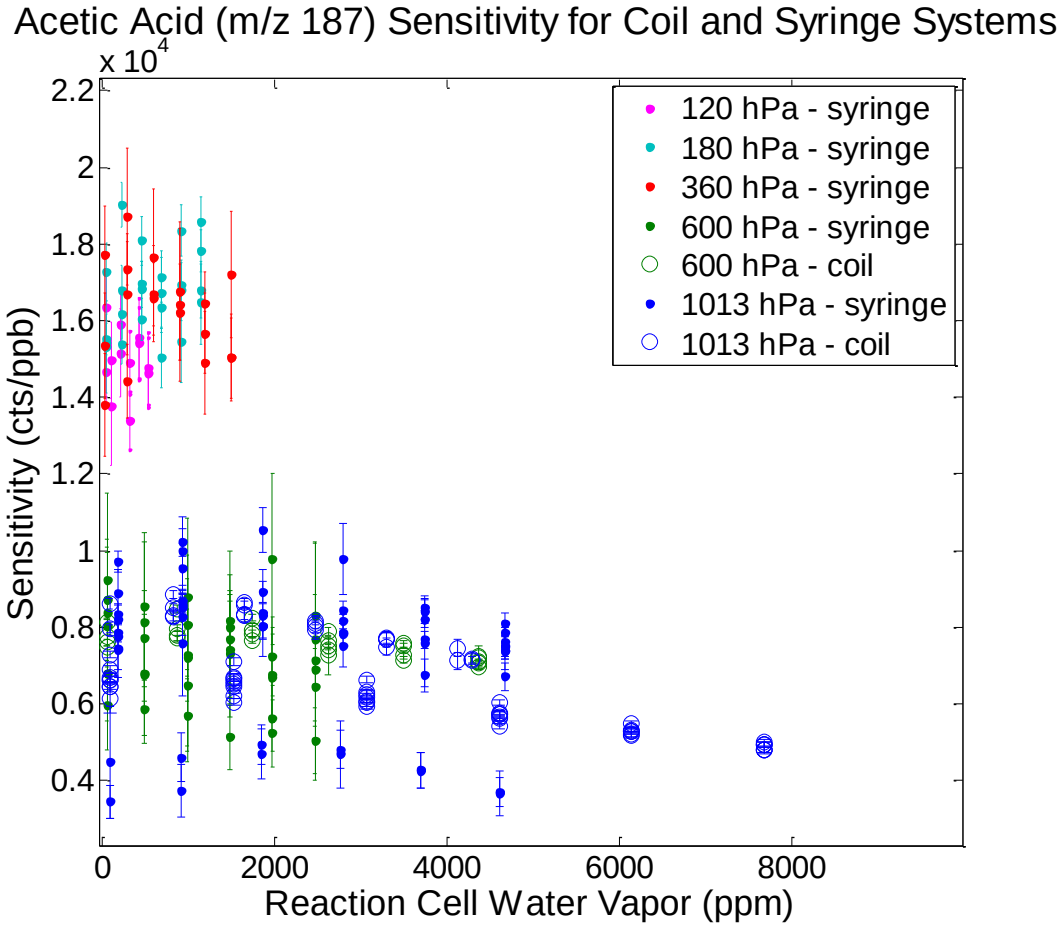

Figure 7: Acetic acid sensitivities as a function of reaction cell water vapor for 120, 180, 360, 600, and 1013 hPa for the coil calibration and one-syringe microfluidic calibration systems with the 0.33% iodomethane reagent gas (Le Breton mixture). The bars represent one standard deviation as calculated in Appendix A.

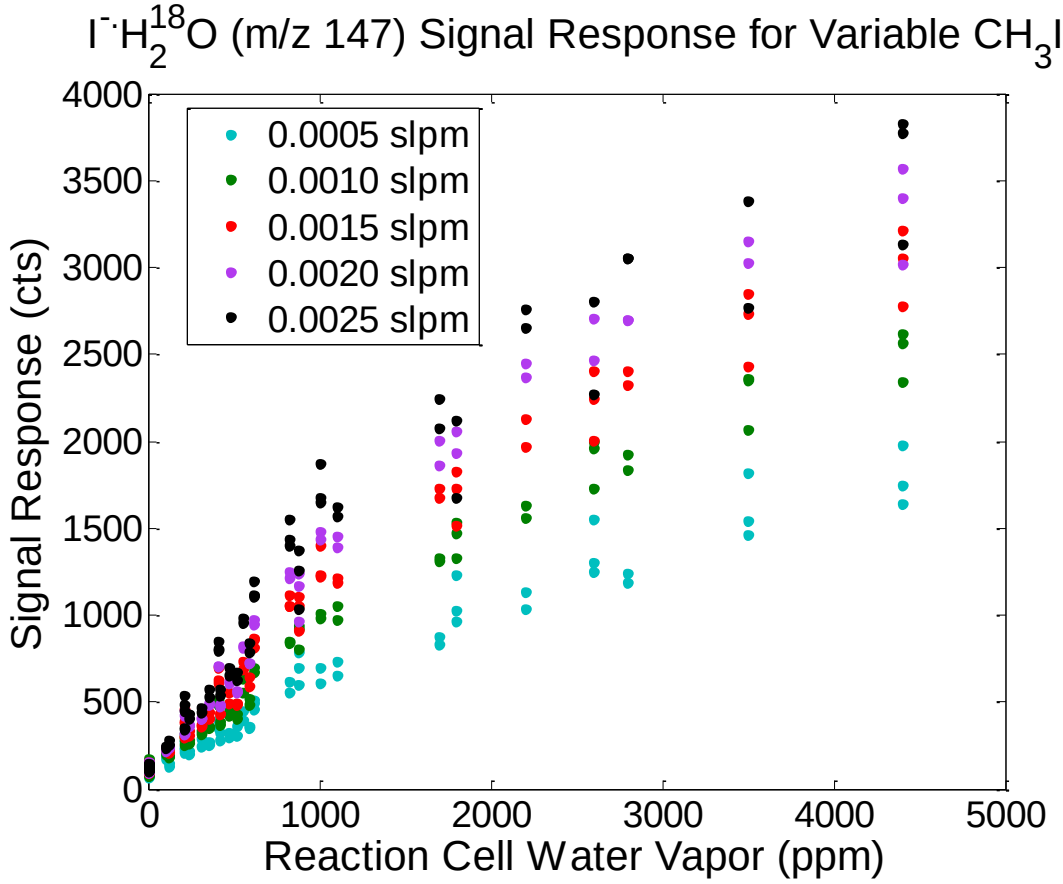

Figure 8: Iodide and water cluster ($I^-•H_2{}^{18}O$) signal response for the five different iodomethane flow rates (0.0005 – 0.0025 slpm) of the 5 ppm iodomethane mixture. Different pressures (120, 180, 360, 600, and 1013 hPa) were tested but are not identified.

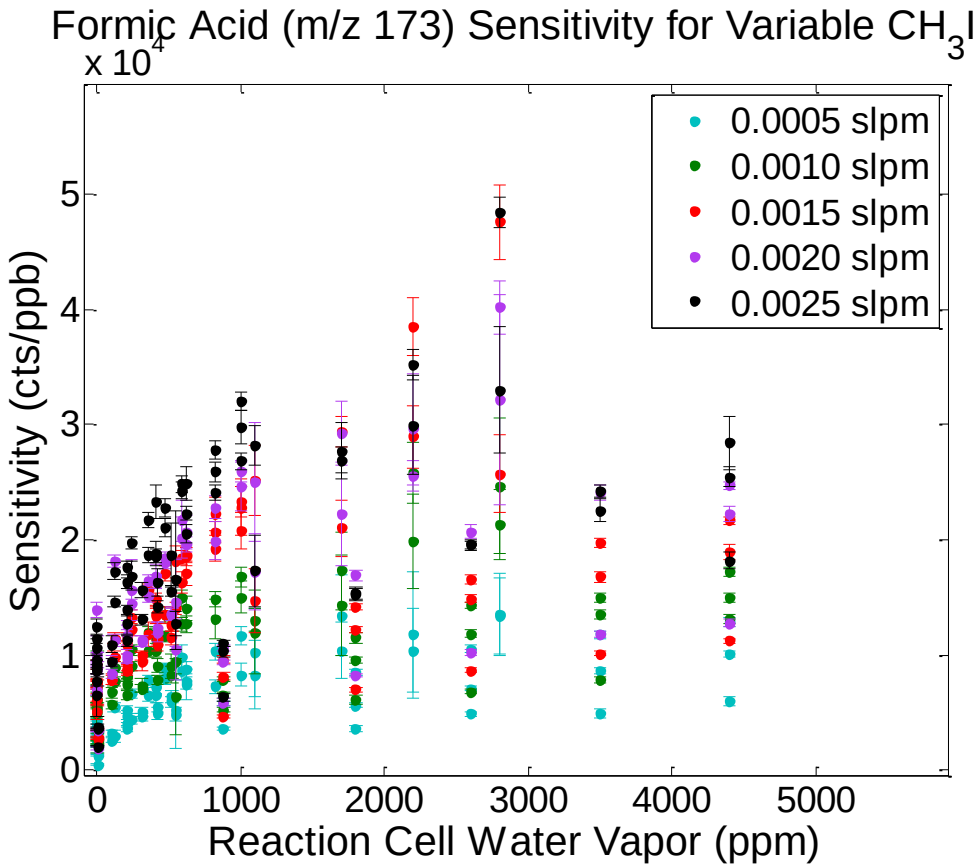

Figure 9: Formic acid sensitivity for the different iodomethane flow rates using the 5 ppm iodomethane mixture. Calibration work at different pressures (120, 180, 360, 600, and 1013 hPa) was performed but are not identified. The bars represent one standard deviation as calculated in Appendix A.

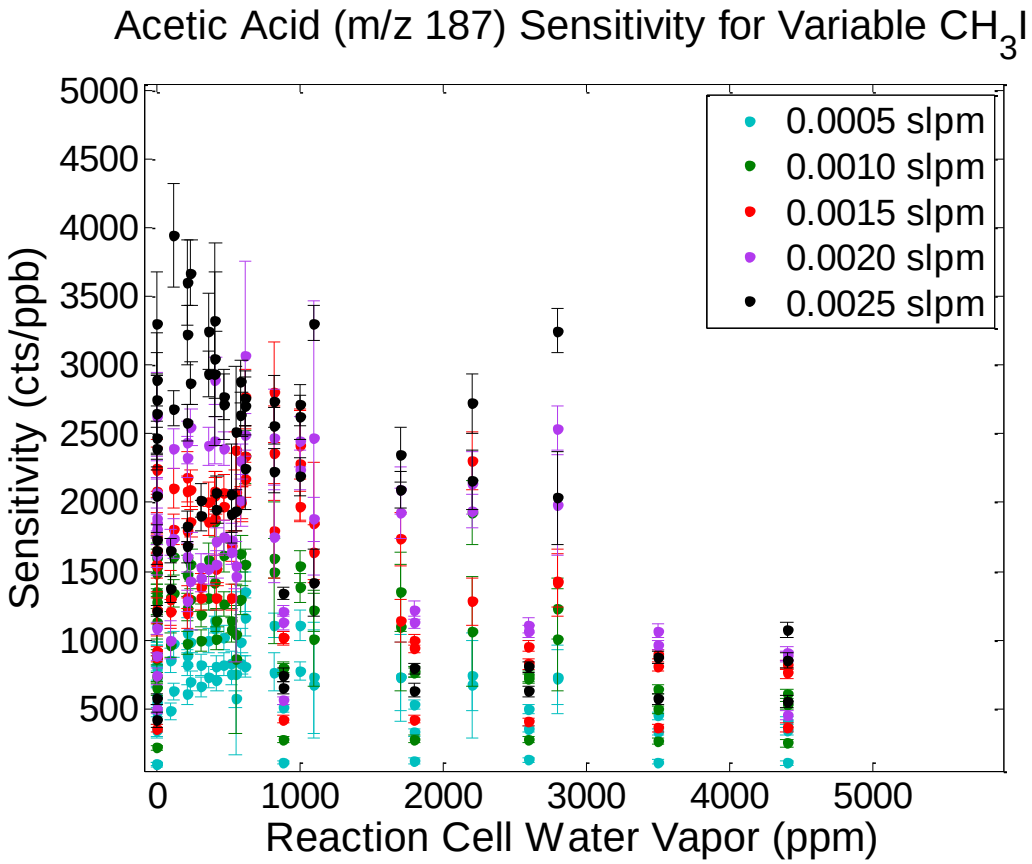

Figure 10: Acetic acid sensitivity for the different iodomethane flow rates using the 5 ppm iodomethane mixture. Calibration work at different pressures (120, 180, 360, 600, and 1013 hPa) was performed but are not identified. The bars represent one standard deviation as calculated in Appendix A.

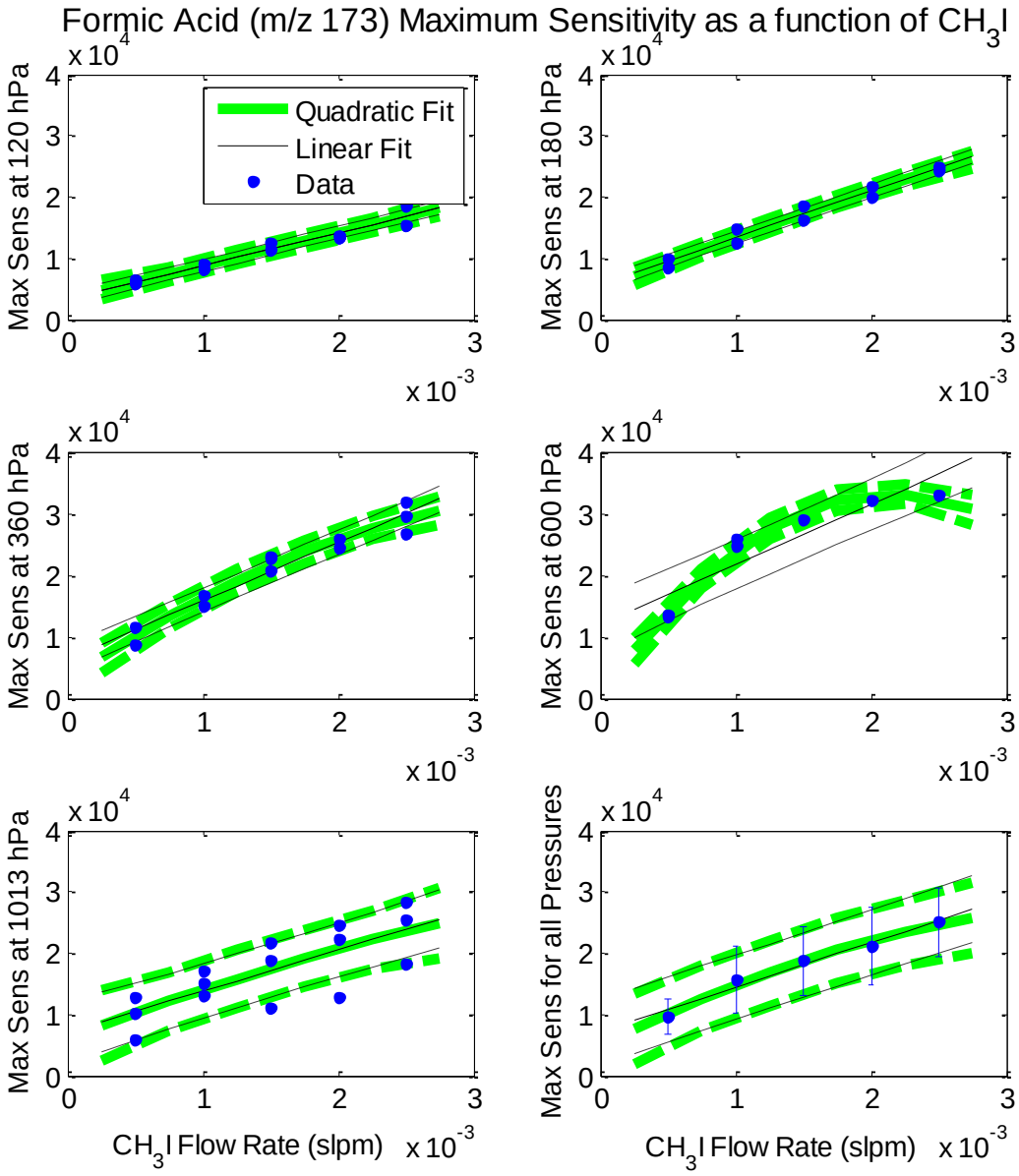

Figure 11: Formic acid maximum sensitivity at each iodomethane flow rate for the 5 ppm mixture regardless of reaction cell water vapor. The black line is the linear fit and 95% confidence interval. The green line is the quadratic fit and 95% confidence interval. The sixth panel (bottom right) is the average maximum sensitivity and one standard deviation regardless of pressures at each flow rate.

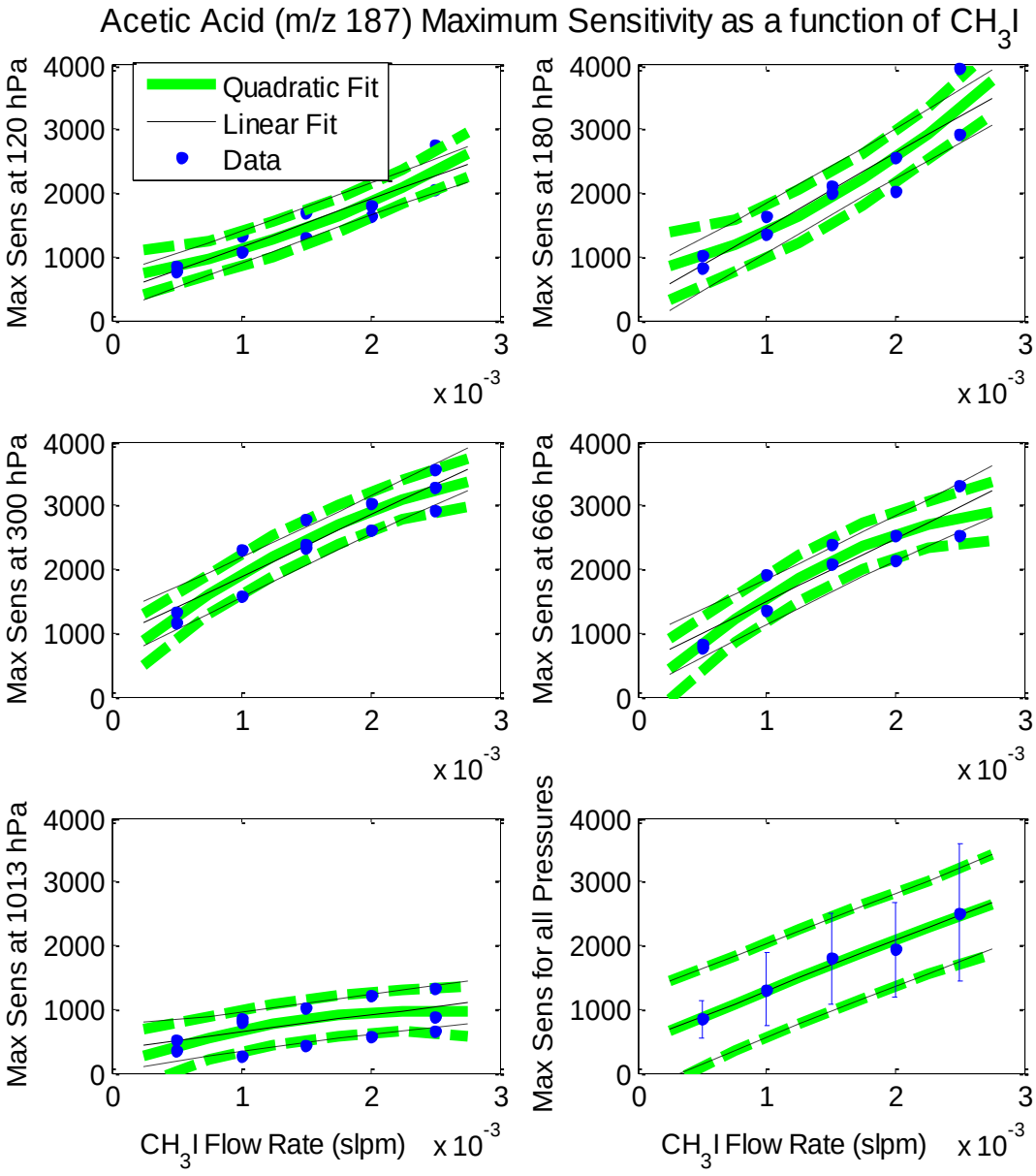

Figure 12: Acetic acid maximum sensitivity at each iodomethane flow rate for the 5 ppm mixture regardless of reaction cell water vapor. The black line is the linear fit and 95% confidence interval and the green line is the quadratic fit and 95% confidence interval. The sixth panel (bottom right) is the average maximum sensitivity and one standard deviation regardless of pressures at each flow rate.

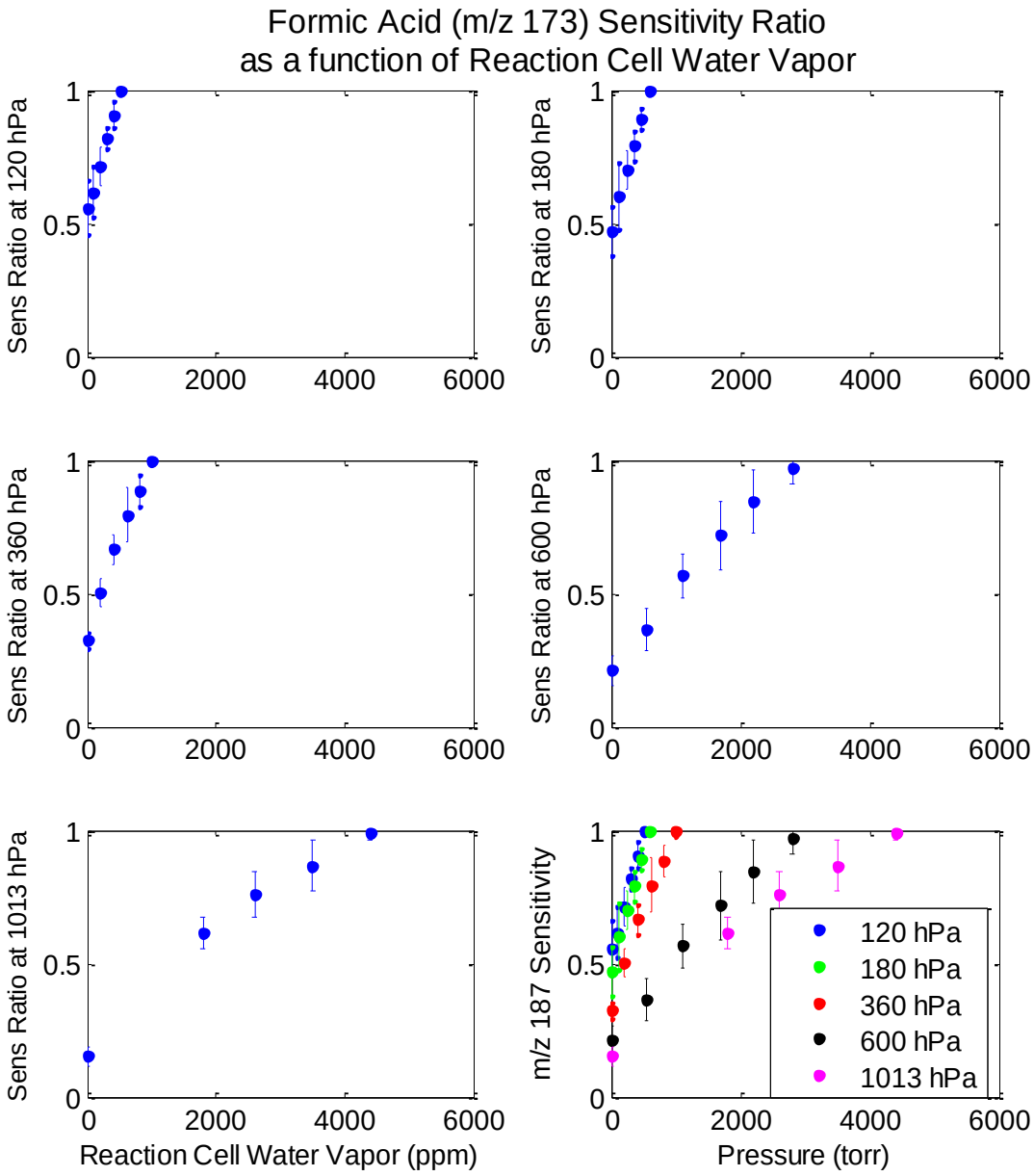

Figure 13: Formic acid sensitivity ratio (sensitivity/ maximum sensitivity) for the 5 ppm iodomethane mixture at 0.0005 slpm and one standard deviation. The sixth panel (bottom right) includes all the sensitivity ratios together identified by pressure.

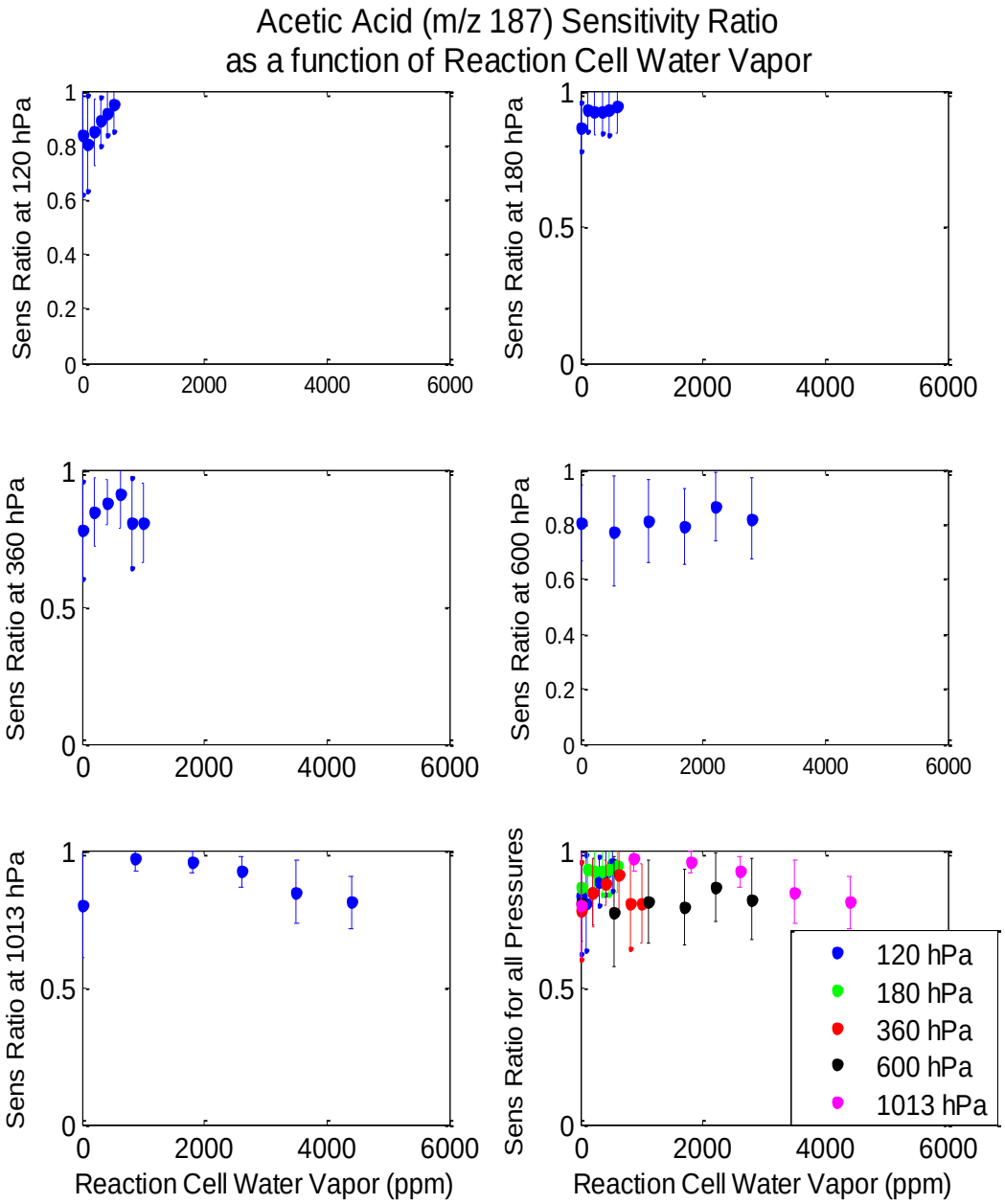

Figure 14: Acetic acid sensitivity ratio (sensitivity/ maximum sensitivity) for the 5 ppm iodomethane mixture at 0.0005 slpm and one standard deviation. The sixth panel (bottom right) includes all the sensitivity ratios together identified by pressure.

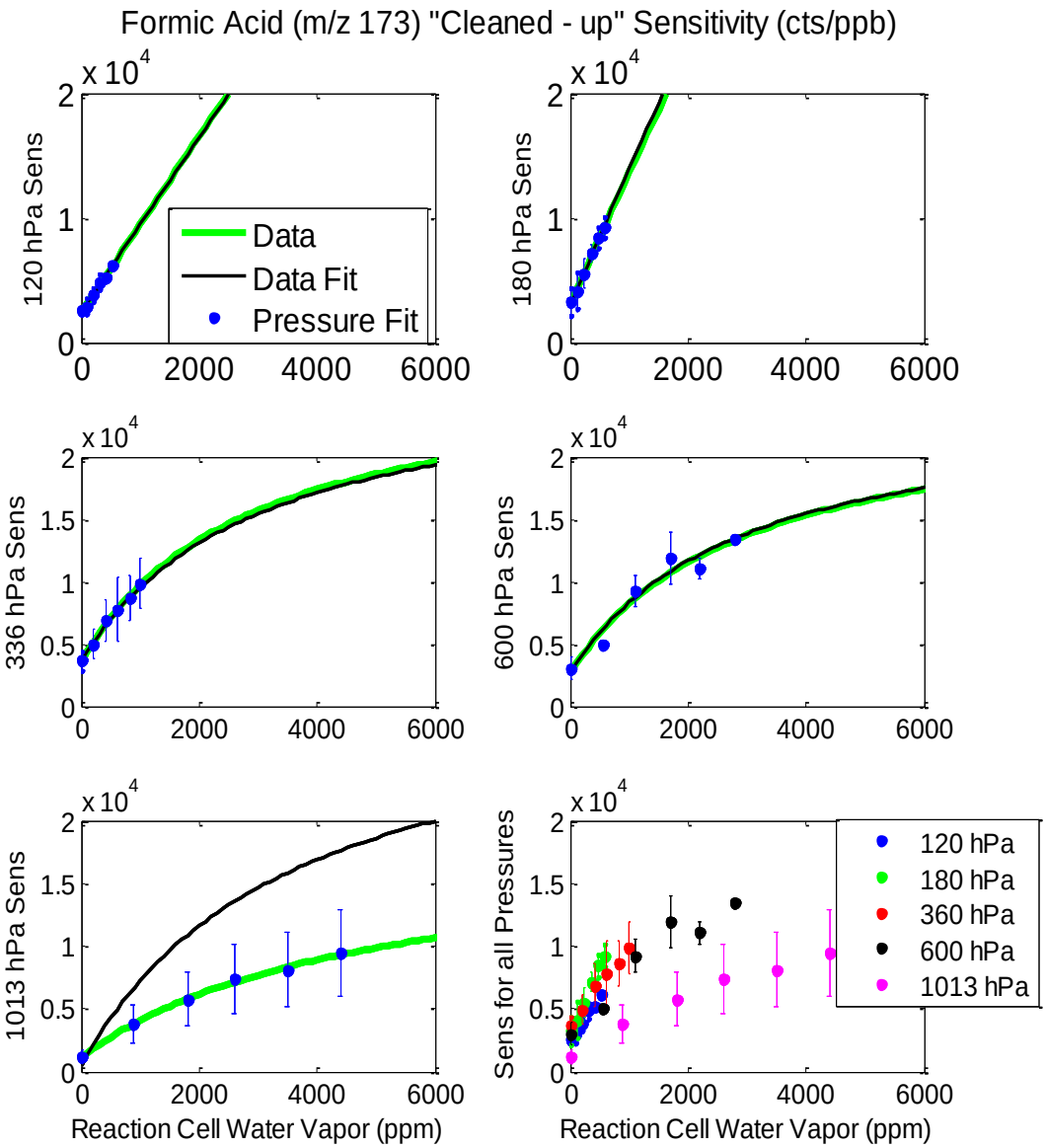

Figure 15: Formic acid "cleaned-up" sensitivity (sensitivity ratio multiplied by the averaged maximum sensitivity) for the 5 ppm iodomethane mixture at 0.0005 slpm. The bars are one standard deviation. The green line is the water only fit and the black line is the water and pressure fit. The sixth panel (bottom right) includes all the sensitivities together identified by pressure.

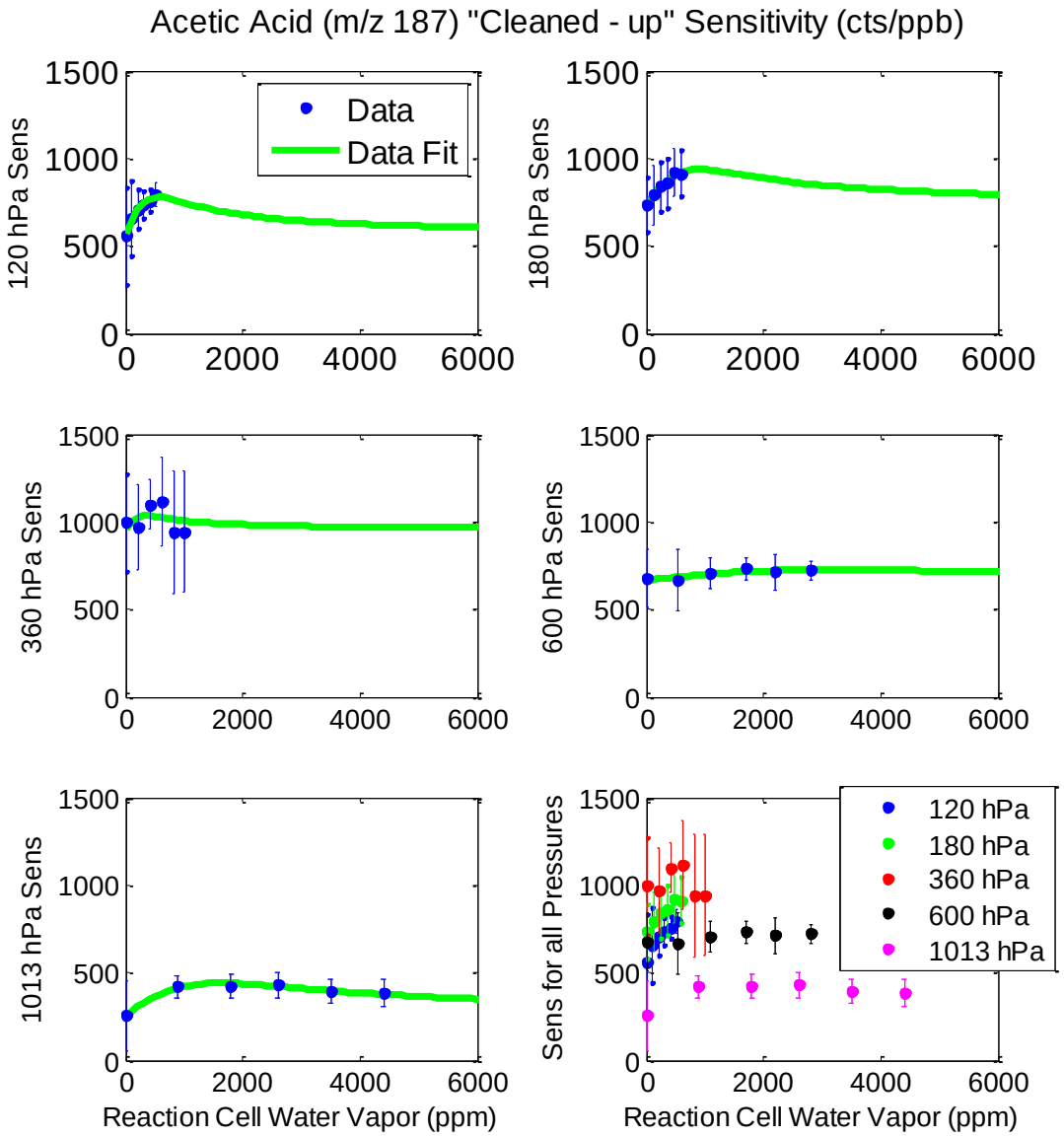

Figure 16: Acetic acid "cleaned-up" sensitivity (sensitivity ratio multiplied by the averaged maximum sensitivity) for the 5 ppm iodomethane mixture at 0.0005 slpm. The bars are one standard deviation. The green line is the water only fit. The sixth panel (bottom right) includes all the sensitivities together identified by pressure.

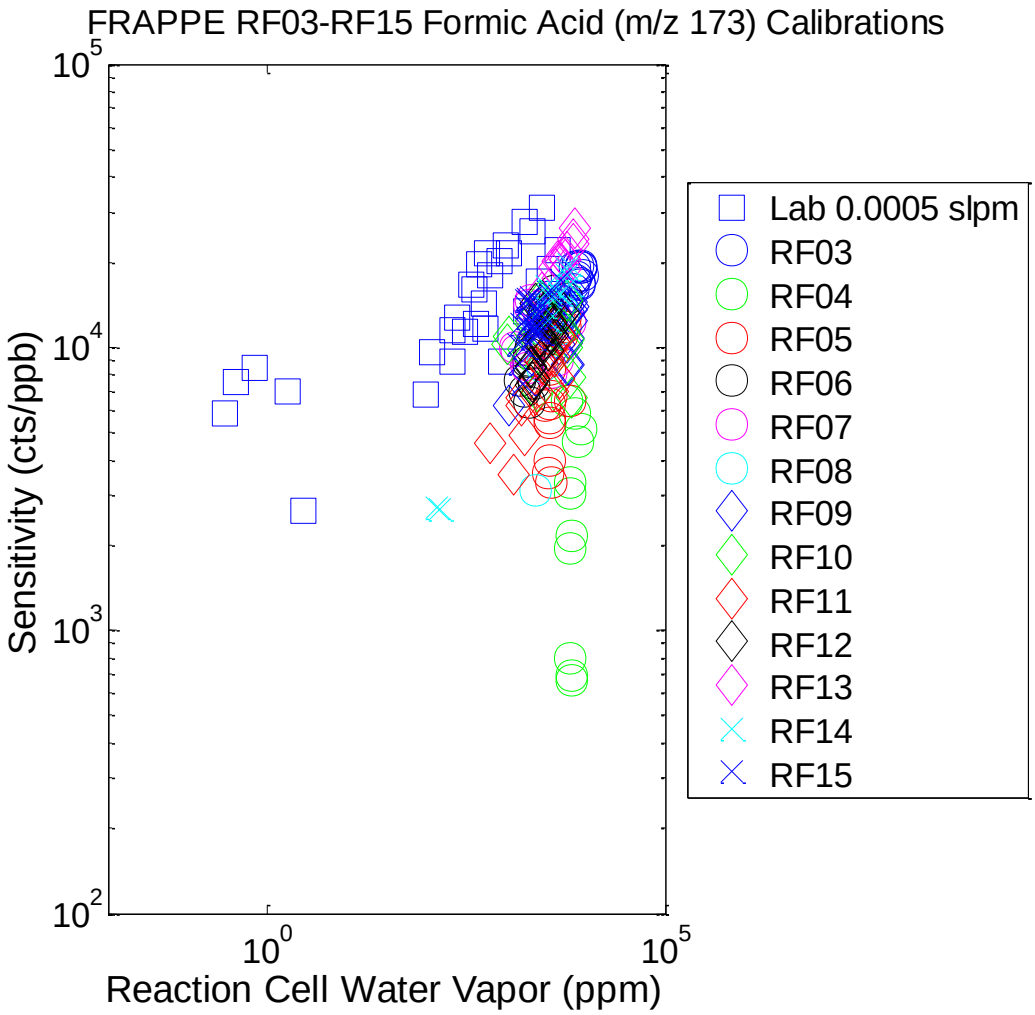

Figure 17: Formic acid sensitivity for FRAPPE in-flight calibrations and laboratory iodomethane calibrations (blue squares). Both FRAPPE and laboratory calibrations used the two-syringe microfluidic set-up with the 5 ppm iodomethane mixture (0.0005 slpm).

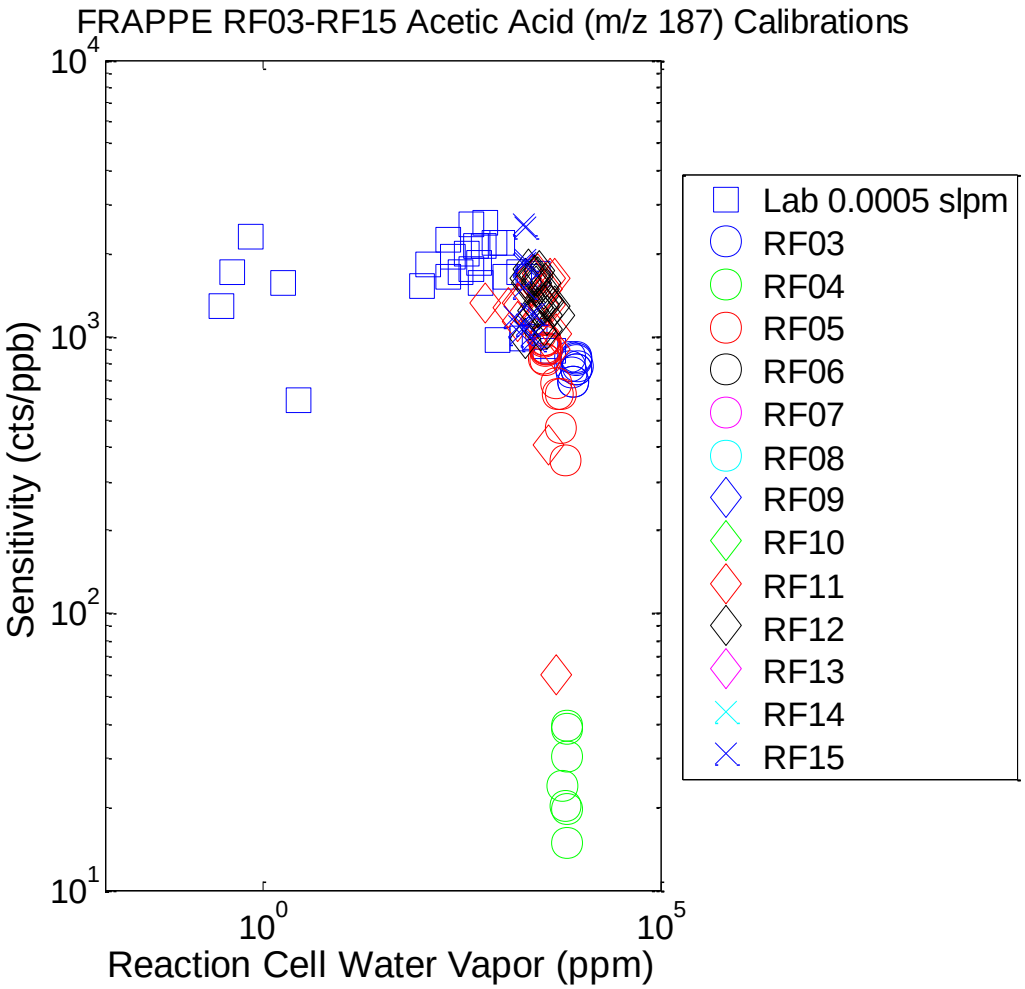

Figure 18: Acetic acid sensitivity for FRAPPE in-flight calibrations and laboratory iodomethane calibrations (blue squares). Both FRAPPE and laboratory calibrations used the two-syringe microfluidic set-up with the 5 ppm iodomethane mixture (0.0005 slpm).

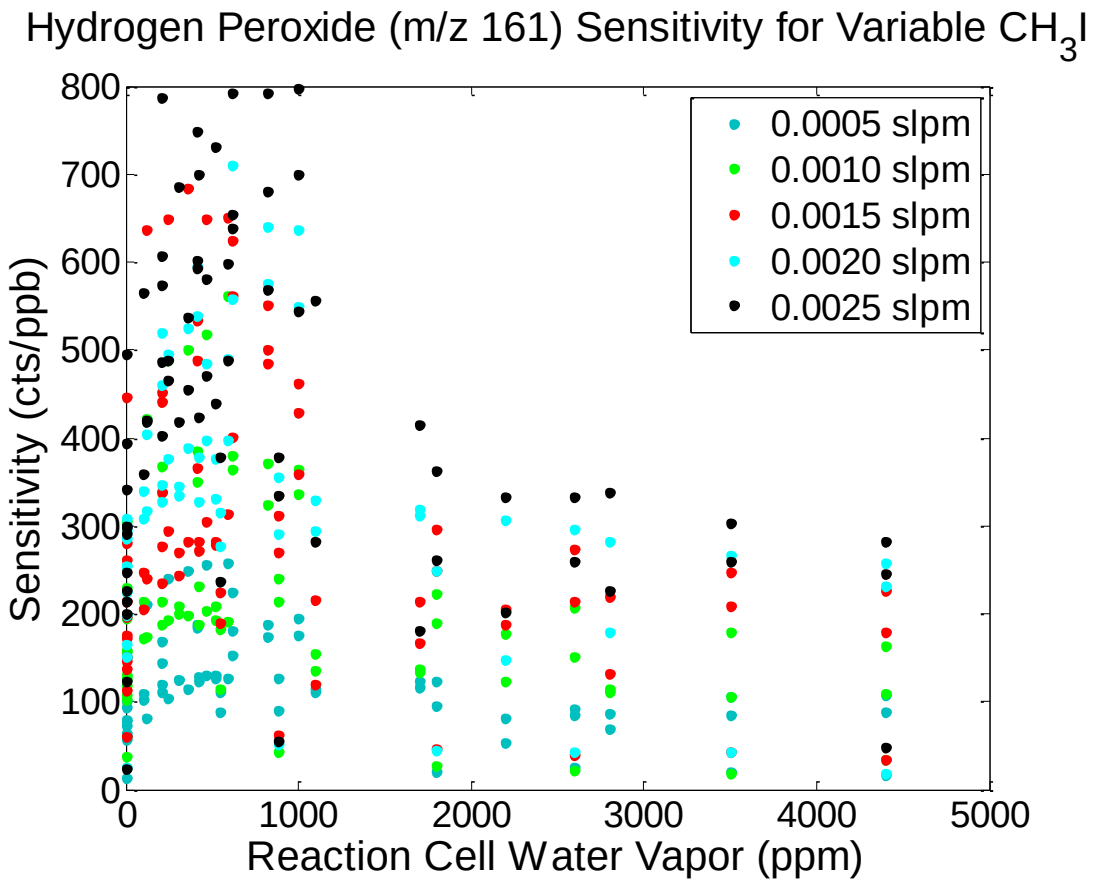

Figure 19: Hydrogen peroxide sensitivity ($I^- \bullet H_2O_2$) for the five different CH_3I flow rates (0.0005 – 0.0025 slpm) of the 5ppm iodomethane mixture. Calibration work at different pressures (120, 180, 360, 600, and 1013 hPa) was performed but are not identified.

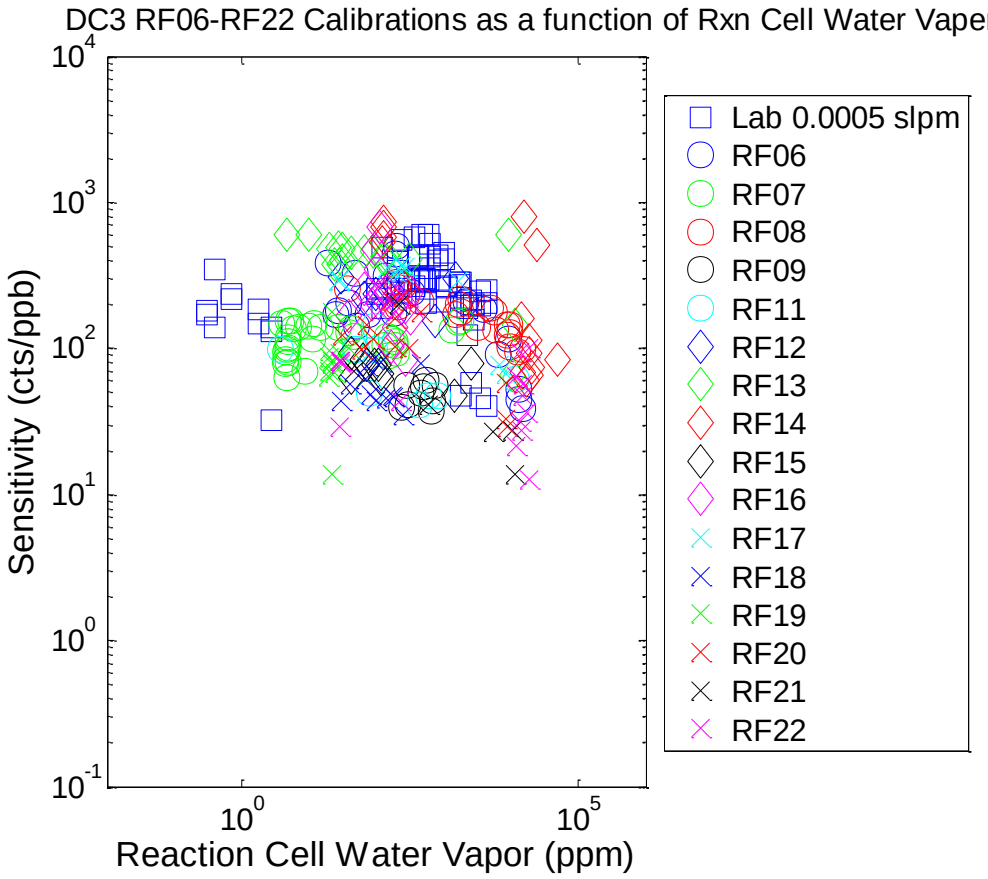

Figure 20: Hydrogen peroxide sensitivity for DC3 in-flight and laboratory CH_3I calibrations (blue squares). DC3 calibrations used the one-syringe microfluidic set-up and the CO_2•O_2 reagent gas. Laboratory calibrations used the two-syringe microfluidic set-up and the 5 ppm iodomethane mixture (0.0005 slpm).

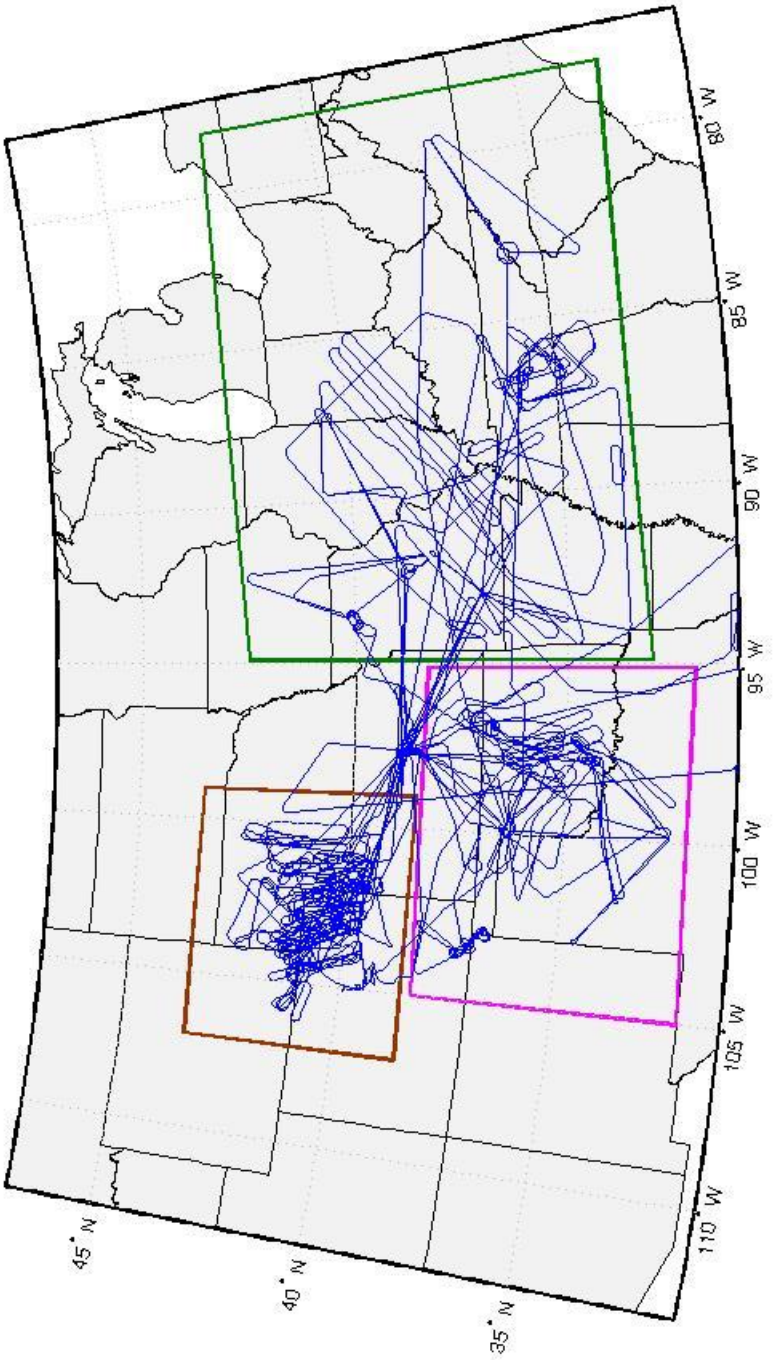

Figure 21: Map of the three DC3 flight domains: Colorado (red), Oklahoma-Texas (magenta), and Eastern region (green)

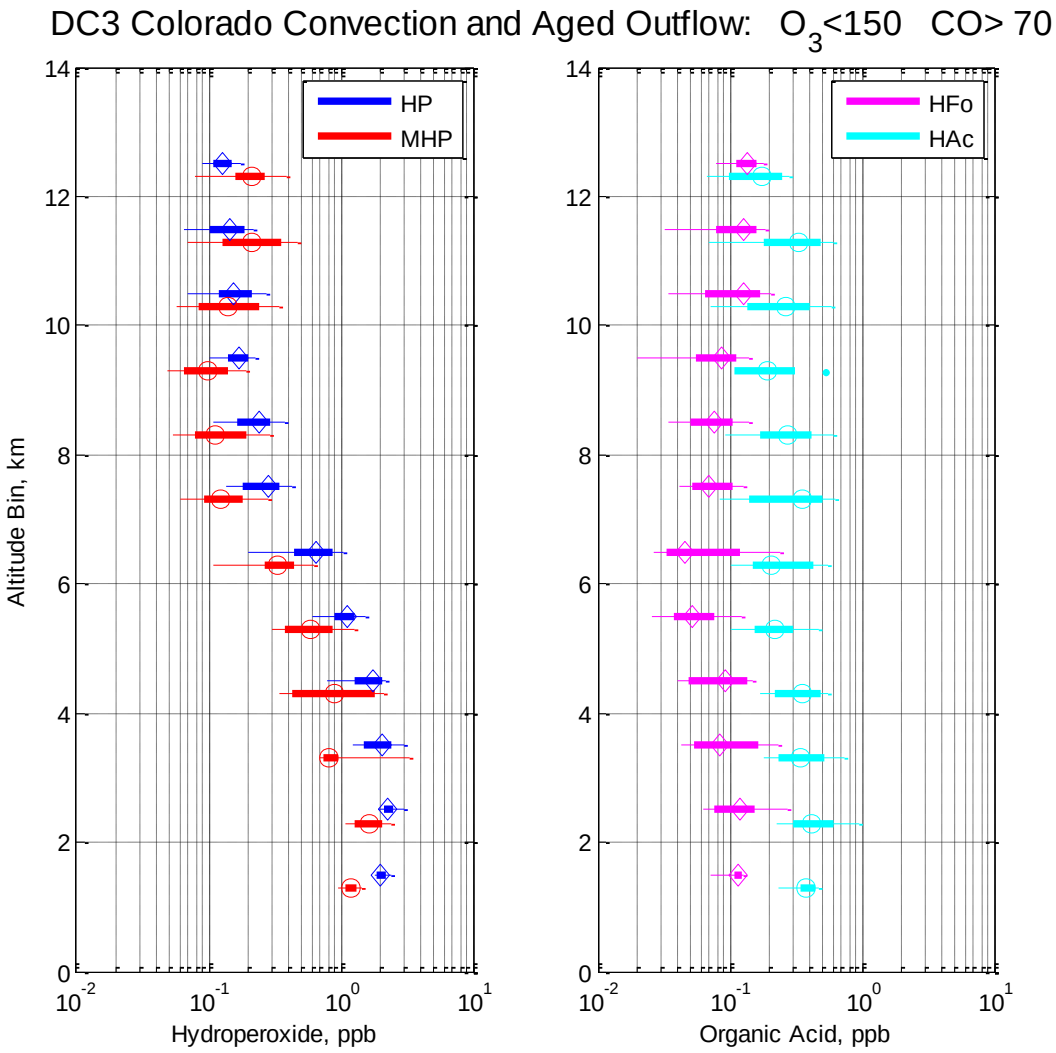

Figure 22: Altitude profile for hydroperoxides (HP – hydrogen peroxide, MHP – methyl hydroperoxide) and organic acids (HFo – formic acid, HAc- acetic acid) for the Colorado region of DC3. All data have stratospherically influenced air removed (O_3> 150 ppb and CO < 70 ppb).

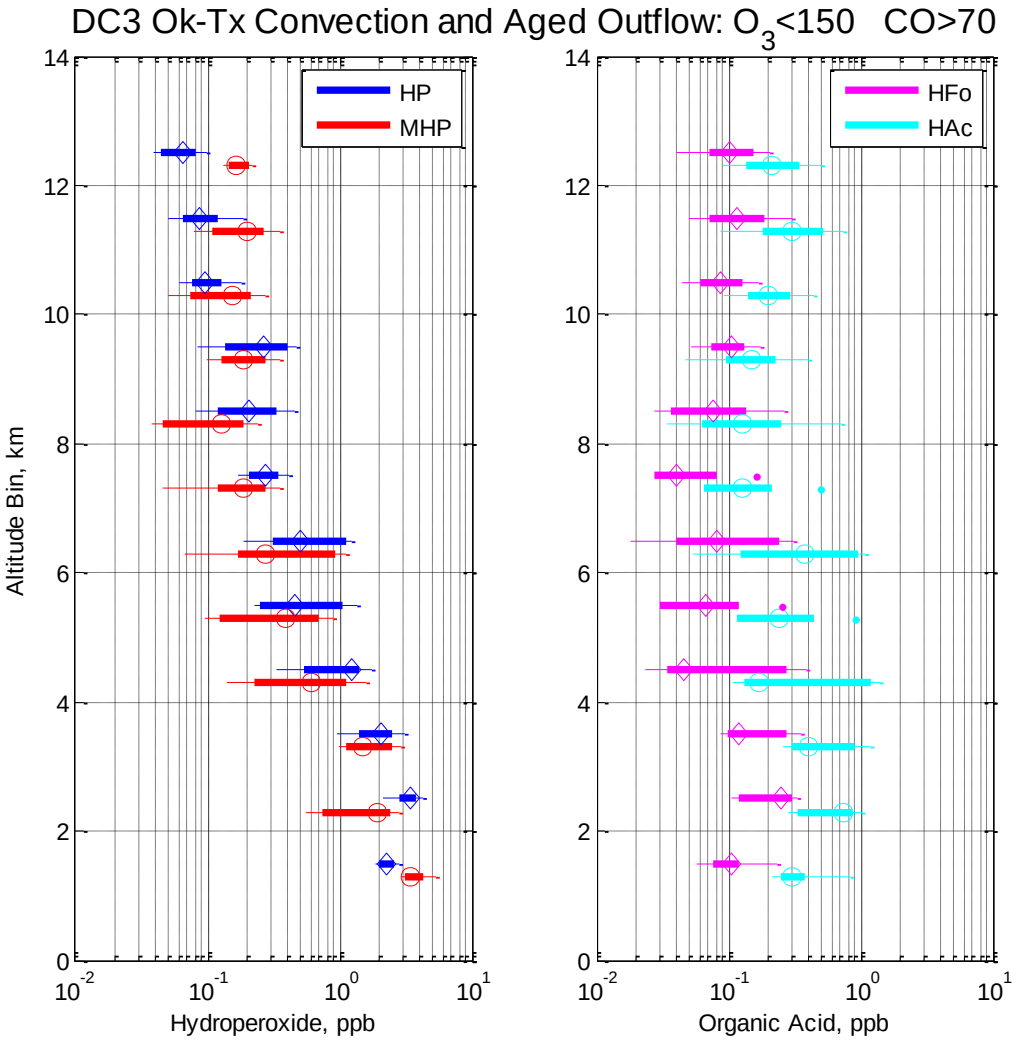

Figure 23: Altitude profile for hydroperoxides (HP – hydrogen peroxide, MHP – methyl hydroperoxide) and organic acids (HFo – formic acid, HAc- acetic acid) for the Oklahoma-Texas region of DC3. All data have stratospherically influenced air removed (O_3 > 150 ppb and CO < 70 ppb).

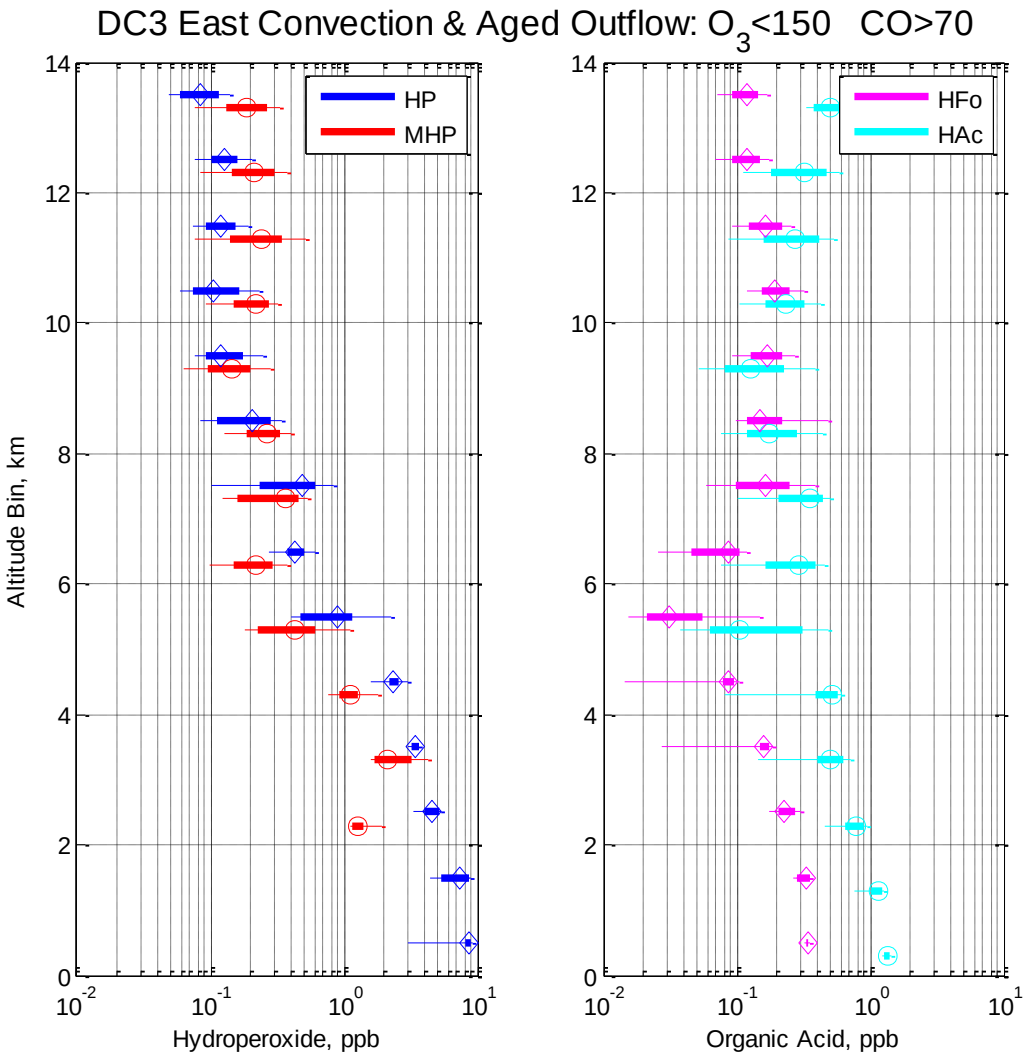

Figure 24: Altitude profile for hydroperoxides (HP – hydrogen peroxide, MHP – methyl hydroperoxide) and organic acids (HFo – formic acid, HAc- acetic acid) for the Eastern region of DC3. All data have stratospherically influenced air removed (O_3 > 150 ppb and CO < 70 ppb).

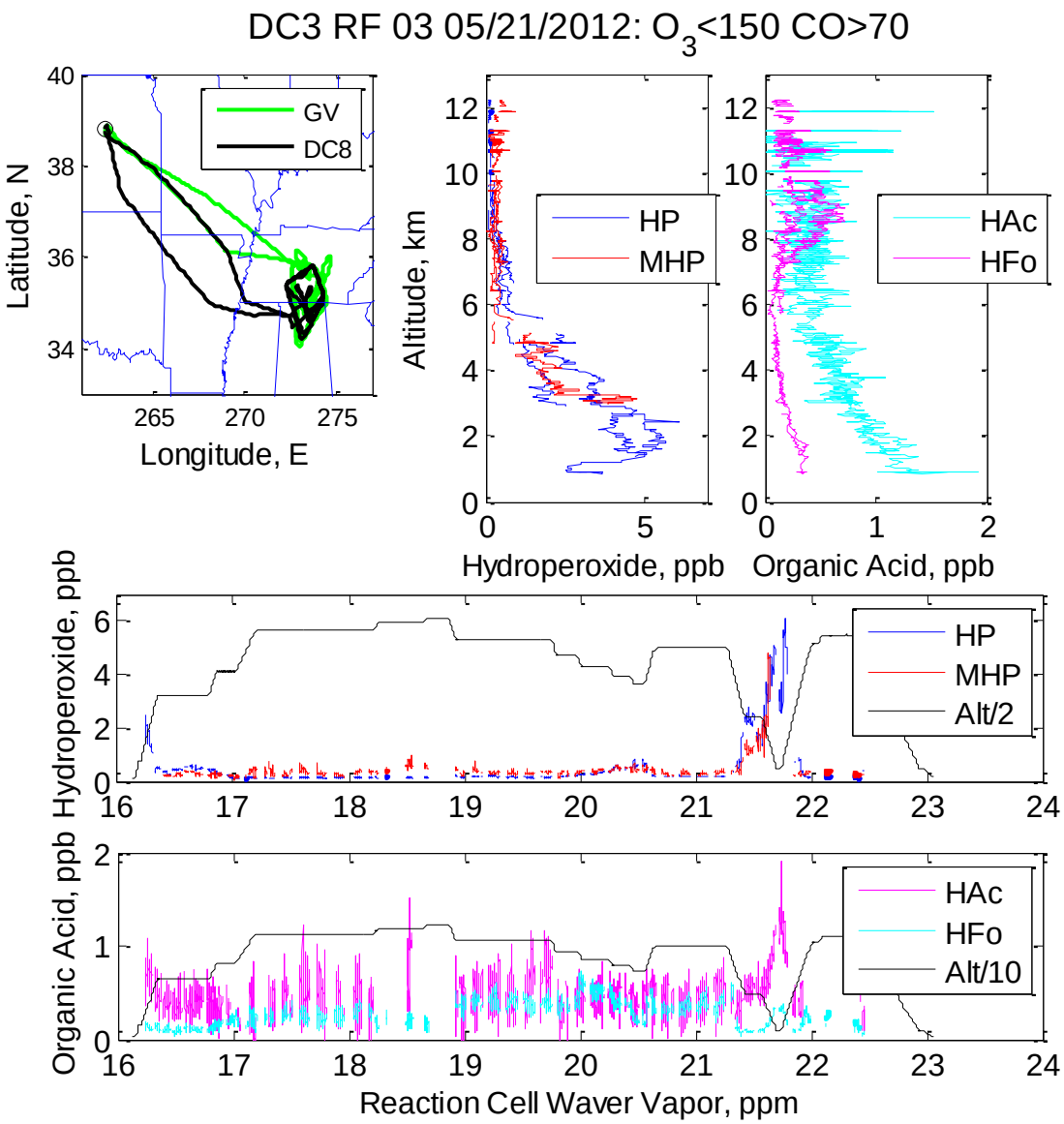

Figure 25: DC3 RF 03 Case Study: the GV and DC8 flight tracks, altitude profiles for the hydroperoxides (HP – hydrogen peroxide, MHP – methyl hydroperoxide) and organic acids (HFo – formic acid, HAc- acetic acid), and times series for the hydroperoxides and organic acids along with the altitude track. All data have stratospherically influenced air removed (O_3 > 150 ppb and CO < 70 ppb).

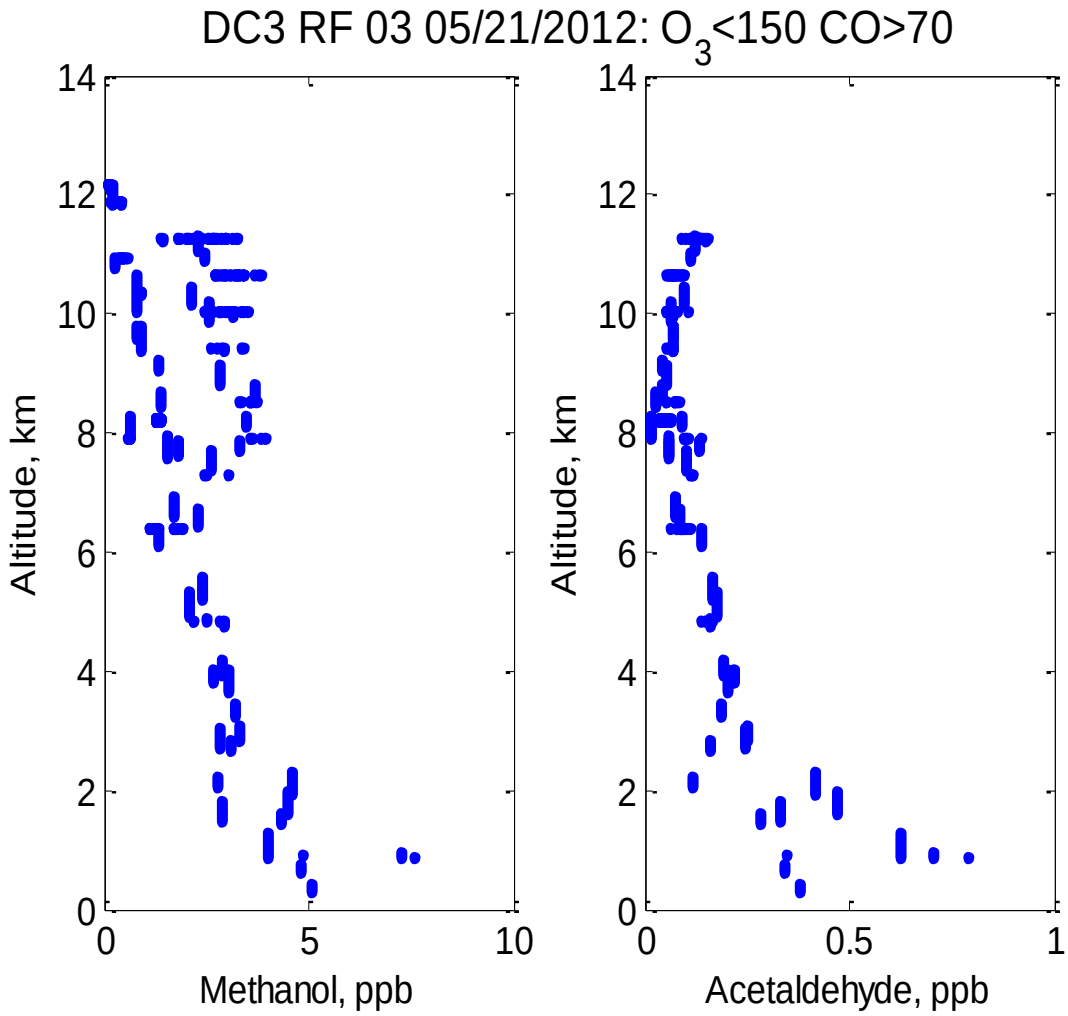

Figure 26: DC3 RF 03 case study: altitude profiles for methanol and acetaldehyde from the TOGA instrument with stratospherically influenced air removed (O_3 > 150 ppb and CO < 70 ppb).

APPENDIX A: ERROR PROPAGATION

The sensitives for the different calibration systems are a function of signal response and reaction cell sensitivity factors. The error propagation has to account for error associated with both the signal response and sensitivity factor. The signal response error results from fluctuations in the signal and is treated as the standard deviation of the averaged counts. The sensitivity factor error comes primarily from instrumental sources (i.e. mass flow controllers). The general error equation (regardless of calibration source) is

$$\delta S = S * \sqrt{\left(\frac{\delta Cts}{Cts}\right)^2 + \left(\frac{\delta X_{rxn\ cell}}{X_{rxn\ cell}}\right)^2} \quad \text{(A1)}$$

where cts is the CIMS raw signal response and $X_{rxncell}$ is the reaction cell sensitivity factor. Both the coil and microfluidic error propagation use the sample flow rate. The error associated with the sample flow rate is

$$\delta F_{sample} = F_{sample} * \sqrt{\left(\frac{\delta F_{N2}}{F_{N2}}\right)^2 + \left(\frac{\delta F_{reag}}{F_{reag}}\right)^2} \quad \text{(A2)}$$

where F_{N2} is the nitrogen flow rate and F_{reag} is the reagent flow rate.

The coil system sensitivity (Eqn 1) error must account for the error associated with the sample flow rate (F_{sample}) and the calibration flow ($F_m = F_c/F_{Aadco}$). It is assumed that the error in the standard preparation is much smaller than the other sources of error and is neglected. It is also assumed that the error in Henry's Law constants are negligible. The coil system reaction cell (Eqn 1) error ($\delta X_{rxncell,\ coil}$) is

$$X_{rxncell,coil} = X_{rxncell,coil} * \sqrt{\left(\frac{\delta F_m}{F_m}\right)^2 + \left(\frac{\delta F_{sample}}{F_{sample}}\right)^2} \quad \text{(A3)}$$

where δF_m is

$$\delta F_m = F_m * \sqrt{\left(\frac{\delta F_T}{F_T}\right)^2 + \left(\frac{\delta F_C}{F_C}\right)^2} \quad \text{(A4)}$$

where F_T is the total flow (Aadco: dry and humidified and calibration (Fc)).

The microfluidic sensitivity (Eqn 2) error ($\delta X_{rxncell,syr}$) needs to account for the sample and excess flow rates. It is assumed that the error in the syringe flow rate is negligible and F_{CIMS} is treated as a "true value".

$$\delta X_{rxncell,syr} = \frac{F_{syr}}{F_{CIMS}} * X_{rxncell,syr} * \sqrt{\left(\frac{\delta F_B}{F_B}\right)^2 + \left(\frac{\delta F_{sample}}{F_{sample}}\right)^2} \quad \text{(A5)}$$

and δF_B is

$$\delta F_B = F_B * \sqrt{\left(\delta F_{sample}\right)^2 + (\delta F_{excess})^2} \quad \text{(A6)}$$

for F_B which is $F_{sample} + F_{excess}$. The two-syringe microfluidic system will be slightly different because there are two reagent gases but the general formula is the same.

BIBLIOGRAPHY

Baasandorj, M., D. B. Millet, L. Hu, D. Mitroo, and B. J. Williams. 2014. "Measuring Acetic and Formic Acid by Proton Transfer Reaction-Mass Spectrometry: Sensitivity, Humidity Dependence, and Quantifying Interferences." *Atmospheric Measurement Techniques Discussions* 7 (10): 10883–930. doi:10.5194/amtd-7-10883-2014.

Barth, M.C., Christopher A Cantrell, William H Brune, Steven A Rutledge, James H Crawford, Heidi Huntrieser, Lawrence D Carey, et al. 2014. "The Deep Convective Clouds and Chemistry (DC3) Field Campaign." *Bulletin of the American Meteorological Society*, December. American Meteorological Society. doi:10.1175/BAMS-D-13-00290.1.

Barth, M.C., S.-W. Kim, W. C. Skamarock, a. L. Stuart, K. E. Pickering, and L. E. Ott. 2007. "Simulations of the Redistribution of Formaldehyde, Formic Acid, and Peroxides in the 10 July 1996 Stratospheric-Tropospheric Experiment: Radiation, Aerosols, and Ozone Deep Convection Storm." *Journal of Geophysical Research* 112 (D13): D13310–34. doi:10.1029/2006JD008046.

Crounse, JD, KA McKinney, AJ Kwan, and P.O Wennberg. 2006. "Measurement of Gas-Phase Hydroperoxides by Chemical Ionization Mass Spectrometry." *Analytical Chemistry* 78 (19): 6726–32.

Díaz-Robles, L. a., J. S. Fu, and G. D. Reed. 2013. "Emission Scenarios and the Health Risks Posed by Priority Mobile Air Toxics in an Urban to Regional Area: An Application in Nashville, Tennessee." *Aerosol and Air Quality Research* 13 (3): 795–803. doi:10.4209/aaqr.2012.07.0165.

Dunlea, E. J., P. F. DeCarlo, a. C. Aiken, J. R. Kimmel, R. E. Peltier, R. J. Weber, J. Tomlinson, et al. 2009. "Evolution of Asian Aerosols during Transpacific Transport in INTEX-B." *Atmospheric Chemistry and Physics* 9 (19): 7257–87. doi:10.5194/acp-9-7257-2009.

EPA. 2009. *EPA Standard Operating Procedure for Coating and Extracting Annular Denuders with Sodium Carbonate*. Research Triangle Park.

Fuzzi, S, and MO Andreae. 2006. "Current State of Scientific Knowledge, Terminology, and Research Needs Concerning the Role of Organic Aerosols in the Atmosphere, Climate, and Global Change." *Atmospheric …* 6: 2017–38.

Hermans, Ive, Pierre Jacobs, and Jozef Peeters. 2007. "The Formation of Byproducts in the Autoxidation of Cyclohexane." *Chemistry - A European Journal* 13 (3): 754–61. doi:10.1002/chem.200601242.

Johnson, Bryan J., Eric a. Betterton, and David Craig. 1996. "Henry's Law Coefficients of Formic and Acetic Acids." *Journal of Atmospheric Chemistry* 24 (2): 113–19. doi:10.1007/BF00162406.

Jones, Benjamin T., Jennifer B.A. Muller, Sebastian J. O'Shea, Asan Bacak, Michael Le Breton, Thomas J. Bannan, Kimberley E. Leather, et al. 2014. "Airborne Measurements of HC(O)OH in the European Arctic: A Winter – Summer Comparison." *Atmospheric Environment* 99. Elsevier Ltd: 556–67. doi:10.1016/j.atmosenv.2014.10.030.

Kawamura, K., L. L. Ng, and I. R. Kaplan. 1985. "Determination of Organic Acids (C1-C10) in the Atmosphere, Motor Exhausts, and Engine Oils." *Environmental Science and Technology* 19 (11): 1082–86. doi:10.1021/es00141a010.

Khare, P, N Kumar, KM Kumari, and SS Srivastava. 1999. "Atmospheric Formic and Acetic Acids: An Overview." *Reviews of Geophysics* 32 (2): 227–48.

Le Breton, M., M. R. McGillen, J. B. a. Muller, a. Bacak, D. E. Shallcross, P. Xiao, L. G. Huey, D. Tanner, H. Coe, and C. J. Percival. 2012. "Airborne Observations of Formic Acid Using a Chemical Ionization Mass Spectrometer." *Atmospheric Measurement Techniques* 5 (12): 3029–39. doi:10.5194/amt-5-3029-2012.

Lee, Ben H., Felipe D. Lopez-Hilfiker, Claudia Mohr, Theo Kurtén, Douglas R. Worsnop, and Joel a. Thornton. 2014. "An Iodide-Adduct High-Resolution Time-of-Flight Chemical-Ionization Mass Spectrometer: Application to Atmospheric Inorganic and Organic Compounds." *Environmental Science and Technology* 48 (11): 6309–17. doi:10.1021/es500362a.

Messer, Benjamin M, David E Stielstra, Christopher D Cappa, Kurtis W Scholtens, and Matthew J Elrod. 2000. "Computational and Experimental Studies of Chemical Ionization Mass Spectrometric Detection Techniques for Atmospherically Relevant Peroxides." *International Journal of Mass Spectrometry* 197 (1-3): 219–35. doi:10.1016/S1387-3806(99)00260-2.

Millet, D. B., M. Baasandorj, D. K. Farmer, J. a. Thornton, K. Baumann, P. Brophy, S. Chaliyakunnel, et al. 2015. "A Large and Ubiquitous Source of Atmospheric Formic Acid." *Atmospheric Chemistry and Physics Discussions* 15 (4): 4537–99. doi:10.5194/acpd-15-4537-2015.

O'Sullivan, Daniel W, Meehye Lee, Birgitta C Noone, and Brian G Heikes. 1996. "Henry's Law Constant Determinations for Hydrogen Peroxide, Methyl Hydroperoxide, Hydroxymethyl Hydroperoxide, Ethyl Hydroperoxide, and Peroxyacetic Acid." *Journal of Physical Chemistry* 100 (8): 3241–47.

Pandis, Spyros, and John Seinfield. 2006. *Atmospheric Chemistry and Physics: From Air Pollution to Climate Change*. 2nd ed. New York: J. Wiley.

Paulot, F., D. Wunch, J. D. Crounse, G. C. Toon, D. B. Millet, P. F. DeCarlo, C. Vigouroux, et al. 2011. “Importance of Secondary Sources in the Atmospheric Budgets of Formic and Acetic Acids.” *Atmospheric Chemistry and Physics* 11 (5): 1989–2013. doi:10.5194/acp-11-1989-2011.

Reiner, Thomas, Ottmar Möhler, and Frank Arnold. 1999. “Measurements of Acetone, Acetic Acid, and Formic Acid in the Northern Midlatitude Upper Troposphere and Lower Stratosphere.” *Journal of Geophysical Research* 104 (D11): 13943–52. doi:10.1029/1999JD900030.

Sander, Rolf. 1999. “Compilation of Henry’s Law Constants for Inorganic and Organic Species of Potential Importance in Environmental Chemistry.” http://www.mpch-mainz.mpg.de/~sander/res/henry.html.

Snow, Julie a., Brian G. Heikes, Haiwei Shen, Daniel W. O’Sullivan, Alan Fried, and Jim Walega. 2007. “Hydrogen Peroxide, Methyl Hydroperoxide, and Formaldehyde over North America and the North Atlantic.” *Journal of Geophysical Research* 112 (D12): D12S07–24. doi:10.1029/2006JD007746.

Talbot, R W, J E Dibb, K I Klemm, J D Bradshaw, S T Sandholm, G W Sachse, J Collins, et al. 1996. “Chemical Characteristics of Continental Outflow from Asia to the to the Troposphere over the Western Pacific Ocean during September-October 1991 : Results from PEM-West A.” *Journal of Geophysical Research* 101 (D1): 1713–25.

Vinegar, Titration of. 2014. “Experiment 11: Titration of Vinegar.” Accessed June 30. http://www.smc.edu/projects/28/Chemistry_10_Experiments/Ch10_Titration.pdf.